~~CONFIDENTIAL~~

Copy 5
RM E57A30

C.2

NACA RM E57A30

NACA

RESEARCH MEMORANDUM

A PRELIMINARY ANALYSIS OF THE MAGNITUDE OF SHOCK LOSSES IN TRANSONIC COMPRESSORS

By Francis C. Schwenk, George W. Lewis, and Melvin J. Hartmann

Lewis Flight Propulsion Laboratory
Cleveland, Ohio

NATIONAL ADVISORY COMMITTEE FOR AERONAUTICS

WASHINGTON
March 29, 1957

~~CONFIDENTIAL~~

UNCLASSIFIED

NACA RM E57A30

NATIONAL ADVISORY COMMITTEE FOR AERONAUTICS

RESEARCH MEMORANDUM

A PRELIMINARY ANALYSIS OF THE MAGNITUDE OF SHOCK LOSSES IN TRANSONIC COMPRESSORS

By Francis C. Schwenk, George W. Lewis, and Melvin J. Hartmann

SUMMARY

The possible shock system associated with the supersonic blade elements encountered in transonic-compressor rotors is reviewed. The variation of the shock shape and location with operating conditions is described qualitatively. A shock configuration is assumed for operation at minimum over-all loss to estimate the magnitude of shock losses.

The minimum-loss data for a large number of transonic-compressor rotors with circular-arc blades are tabulated, and the shock losses are estimated in most cases to be from 0.35 to 0.55 of the over-all blade-element losses when the inlet relative velocities are sonic or greater. In many cases, estimated surface Mach numbers are high and have a very large effect on the magnitude of shock loss. Large shock losses can be obtained even at relatively low supersonic inlet relative Mach numbers when the surface Mach number is high. The Mach number levels obtained indicate that flow separation probably always occurs at the point of shock - boundary-layer interaction on the blade suction surface. The profile losses are approximated by the difference in measured over-all blade-element loss and the estimated shock loss. Several parameters that may be indicative of profile loss are considered, but no good correlation can be obtained with the data used in this preliminary study. Whereas the diffusion factor developed for subsonic flow does not apply to this type of flow configuration, the profile losses are reasonably close to the previously obtained band. Estimation of the profile loss by the use of the diffusion factor must be considered somewhat tentative and should not be extended appreciably beyond the range of data used in this investigation.

INTRODUCTION

For the design of high-pressure-ratio high-mass-flow axial-flow-compressor stages, accurate information on the losses in relative total pressure occurring in the blade rows is required to predict design-point

performance. Reference 1, for example, shows the importance of accurate design loss values through a discussion of actual and design performance of a transonic-compressor rotor having a design corrected tip speed of 1300 feet per second. Gross efficiency or loss values generally do not suffice, because radial variations in losses (or entropy) occurring in a blade row enter the radial-equilibrium calculation of velocity and angle variations downstream of the blade row (ref. 2). These variations critically affect the performance of a high-pressure-ratio stage and succeeding blade rows as well. The optimization of axial-flow-compressor designs is particularly important in the supersonic-aircraft propulsion field. For such a study, knowledge of the factors that influence losses is required not only at the design point but also at off-design conditions.

Subsonic-compressor design procedures have been based on the blade-element approach (refs. 3 and 4), and two-dimensional-cascade data supplemented by rotor test results were the basis for selection of blades and relative total-pressure-loss coefficients for each blade element. Some early experiments with transonic axial-flow-compressor rotors (refs. 5 to 9) showed that, for inlet relative Mach numbers up to 1.1, shock effects evidently were small, and the transonic compressor appeared as an extension of subsonic-compressor experience (ref. 4). That is, blade-element theory applied, and the measured minimum loss levels depended on blade-loading parameters such as diffusion factor (ref. 10) with no measurable effects of inlet relative Mach number. Of course, the blade sections used in the transonic compressors were different from conventional subsonic airfoils. For example, one successful airfoil is the double-circular-arc airfoil (refs. 7 to 9).

Some recent results of testing compressors having inlet relative Mach numbers up to 1.3 (refs. 1, 11, and 12) showed a departure from previous transonic-compressor experience in that the measured minimum losses fell above the range of the diffusion-factor correlation of reference 10. Similar results were also found in tests of low-solidity (low chord-to-spacing ratio) compressors in which the inlet relative Mach numbers were 1.1 or lower (refs. 13 and 14). As reported in the preceding investigations, these compressors probably represent cases in which the effects of shock waves were great enough to cause the departure from subsonic- and earlier transonic-compressor experience.

The results of references 1 and 11 to 14 lead to some basic conclusions: (1) Certain phases of the subsonic approach to compressor design need modification in the transonic regime; (2) a study of the flow through transonic blade rows is required to learn the relative magnitude of factors that affect losses; and (3) a new or at least a modified design loss variation is required.

This report presents some ideas on the type of flow field that may exist in a transonic axial-flow compressor. Basically, the blade-element

approach is retained, and the possible shock- and expansion-wave configurations for a compressor cascade are considered. Based on this study, the report endeavors to establish a simple shock-wave model that will approximate the shock loss at the design or minimum-loss incidence angle. Besides this, the model will provide a basis for studies of the viscous effects on the blade surface.

ANALYSIS OF FLOW IN TRANSONIC-COMPRESSOR BLADE ELEMENTS

Understanding the flow phenomena and determining correlative parameters for the losses in total pressure in transonic compressors require a knowledge of the flow configuration. The actual physical situation in a compressor is so complex that it almost defies description and makes a quantitative treatment nearly impossible without simplifying assumptions. Thus, for the study of compressor losses, a flow model is usually constructed by simplifying the actual flow field in the hope that the model will closely represent the physical situation and provide an understanding of the important sources of and factors which cause the losses.

Description of Flow Model

The flow model assumed herein is two-dimensional and similar to the blade-element approach usually employed in studies of compressors (ref. 3). Such a model rules out consideration of the flow phenomena in the blade end regions depicted in reference 15. As indicated in some of the analyses of transonic axial-flow compressors (refs. 1 and 11 to 14), the effects of shock waves can have some influence on the observed blade-element losses; therefore, the flow model must allow for the presence of shock waves to be more general than usual blade-element theory.

Before proceeding with a discussion of the shock waves, it is important to consider the assumption of two-dimensional flow, since it is expected that the mixed supersonic and subsonic flow fields in a transonic compressor will be more sensitive to three-dimensional effects than a completely subsonic flow. The two-dimensional-flow hypothesis simplifies the analysis greatly and allows for the comparison of transonic blade-element data with subsonic compressor and cascade data. Through such comparisons, it may be possible to test the hypothesis and to discover situations in which three-dimensional effects are important enough to be considered.

Shock-wave configurations. - Shock-wave configurations for cascades of blades are shown in references 16 to 18. The necessary extensions and modifications to the flow model for transonic-compressor blade elements are discussed in this section.

The shock pattern in a supersonic cascade of compressor blades consists of two parts, as shown in figure 1. The first is that portion of a shock wave contained in the blade passage (from blade suction surface to stagnation streamline) and will be referred to as a passage shock; the shape and location of this passage shock depend on the blade geometry and the operating conditions at a given relative Mach number. The second is that portion of the shock extending from stagnation streamline to infinity upstream of the stagger line and will be referred to as a bow wave; the location and strength of the bow wave depend on blade leading-edge thickness and operating conditions at a given relative Mach number. As shown in figure 1, the bow waves are normal to the flow at the stagnation streamline and approach the slope of a Mach line for the upstream conditions.

The shock-wave configuration is shown in detail in figure 2. The entering flow (a) encounters the shock wave at the point b, where the wave is normal to the stagnation streamline. The portion of the shock wave near the stagnation streamline is a strong wave, and the flow is reduced to subsonic relative velocities. The flow is then expanded around the leading edge of the rotor blade (c) to rather high supersonic velocities. The first expansion wave (c-c') represents the flow at a Mach number of 1.0. The final expansion wave shown originating at the leading edge (c-c") is the Mach line flow as expanded parallel to the suction surface at the leading edge. The flow then continues to accelerate and flow parallel to the suction surface, and the expansion waves that intersect the bow wave reduce the shock strength and cause the bow wave to become a Mach line.

The flow along the next stagnation streamline (d) can now be followed through the flow field established by the lower blade. The stream is deflected upward slightly at the point e as it passes through the bow wave, depending on the slope of the bow wave at this point. The streamline is then deflected downward by the expansion system (e to f). The flow direction is thus established by the expansion system that originates on the suction surface of the previous blade. This stagnation streamline then encounters the bow wave at the point f, and the flow at the leading edge of the next blade (g) is similar to that on the lower blade. As noted on the figure, a value h is assigned to the deflection distance of the stagnation streamline from a continuation of the blade mean camber line. The deflection h of this streamline varies with the contained supersonic flow field.

In order to maintain identical conditions entering each blade of the blade row, the compression in a given bow wave and the expansion system that passes ahead of the next bow wave (fig. 2) must be of equal strength. Thus, the properties of the gas along each bow wave and the entrance conditions are the same for each blade.

Figures 1 and 2 present the shock configurations for a given operating condition. It is expected that changes in operating conditions will alter the shock waves from those shown. This subject is considered later.

Conditions downstream of cascades of blades. - As in studies of low-speed-cascade flow (ref. 19), the nature of the flow at the outlet of a high-speed blade row can be discussed. For comparison purposes, a typical variation in total pressure downstream of low-speed cascade is shown in figure 3. Defined wake and free-stream regions are indicated. The total-pressure-loss coefficient $\bar{\omega}$ is defined as

$$\bar{\omega} = \frac{P_{2,id} - \bar{P}_2}{P_1 - p_1} \qquad (1)$$

where symbols are defined in appendix A. The numerator of equation (1) is the difference between the ideal outlet total pressure and the mass-averaged total pressure $\bar{P}_2$. (The ideal outlet total pressure equals the inlet total pressure for a stationary blade row.) For low-speed compressor rotors, it is assumed that the circumferential variations of relative total pressure at the outlet of a blade row are as shown in figure 3. Data computed from hot-wire-anemometer measurements outside the rotor housing boundary-layer region (ref. 15) support this assumption for a rotor blade element operated with inlet relative Mach numbers equal to approximately 0.8.

On the basis of the shock configurations given in figures 1 and 2, a variation of relative total pressure downstream of a rotor blade element can be deduced for the case of supersonic inlet relative Mach numbers. The passage shock (f to f' in fig. 2) decelerates the flow from supersonic to subsonic velocities, and therefore some losses in total pressure are expected from this shock wave. Furthermore, since the Mach number upstream of the passage shock varies along the wave, a circumferential variation in outlet relative total pressure in addition to the blade wakes is expected. Figure 4 illustrates the passage shock loss qualitatively. Also shown in figure 4 is the complete variation in outlet total pressure including blade wakes. Such variations have been observed in unpublished data taken at the NACA Lewis laboratory with the hot-wire anemometer. Loss coefficients (eq. (1)) determined for rotors having supersonic inlet relative Mach numbers, of course, represent the circumferential variation of total pressure in figure 4 as some average loss in total pressure. The problem, then, is to separate the over-all loss coefficient into the major constituents: the shock losses and the losses due to viscous effects on the blade surfaces.

Variations in the Flow Model with Operating Condition

The flow model, in particular the shock configuration, has been described for one operating condition. Variations in operating conditions will now be discussed to indicate, at least qualitatively, that the flow model will show some of the trends observed in compressor tests. In addition, this discussion will provide a basis for establishing the shock configuration for a particularly important operating condition (maximum-efficiency or design operation of a blade element).

Typical performance characteristics. - Before proceeding with a discussion of the flow model at various operating conditions, it will be of some help to consider the performance characteristics of a typical compressor rotor row operating with supersonic inlet relative velocities over a portion of the blade span (fig. 5(a)). Operation with constant blade speed will be discussed. Within the limits imposed by a test rig, a rotor will exhibit choking at low back pressures. Rotor choking is identified as the condition for which changes in back pressure can occur with no alteration of the rotor inlet flow (point A, fig. 5(a)). Up to a certain point, then, increasing the back pressure above the lowest value available will cause increasing total-pressure ratio and compression within the rotor at a nearly constant weight flow. At some point (B, fig. 5(b)), a maximum rotor efficiency is obtained. At higher back pressure (point C, fig. 5(c)), more compression will occur within the rotor and the weight flow will decrease until further increases in back pressure may be inadvisable because of the appearance of stalled or unstable flow.

Changes in shock-wave configuration with operating condition. - The shock-wave configuration for very low back pressures (rotor choking) is shown in figure 5(a). Since very little compression is required over the blade row, the passage shock wave moves back along the suction surface toward the trailing edge and becomes oblique to the flow. The bow wave is close to the leading edge of the blade; the displacement upstream is due mainly to the leading-edge thickness. For operation with low back pressure and high weight flow, the inlet flow is parallel to or at a slight negative incidence relative to the suction surface. In addition, the pressure surface creates only a small deflection of the stream, so that a supersonic region may form on the pressure side of the blade. Therefore, there is a possibility of a shock and boundary-layer interaction on the pressure surface. The pressure-surface shock wave may be induced by either the back-pressure requirements or the coalescence of compression waves produced by a concavity of the pressure surface.

The Mach number along the suction surface upstream of the passage shock wave becomes very high because of the large amount of supersonic turning, and flow separation may occur and cause a forked shock wave. In some cases, depending on the element geometry and three-dimensional aspects of the flow, the passage shock wave may pass entirely behind the blade row at low back pressures.

Now consider the effect on the flow model as the back pressure is increased (fig. 5(b)) so that the upstream conditions, weight flow, and the bow wave do not change significantly. The downstream pressure increase moves the shock wave forward along the suction surface in order that the necessary compression can occur. Operation as shown in figure 5(b) would represent maximum pressure ratio at maximum weight flow (choke) for a compressor rotor. As the back pressure is increased further (fig. 5(c)) it is necessary that the passage shock and bow wave move away from the leading edge of the blades to achieve the required static-pressure rise. The compression upstream of the leading edge increases and causes an increased incidence angle. Thus, the flow model allows a range of operation similar to that experienced in transonic-compressor rotors.

Losses

The basic purpose of constructing a flow model is to make possible the determination of the flow variations with operating conditions and the factors affecting losses. Two sources of shock loss can be considered, the bow wave and the passage shock. Closely associated with the passage shock wave is the loss due to the shock - boundary-layer interaction and subsonic diffusion from the passage shock to the discharge conditions. These losses are referred to as the profile losses, since they arise mainly from the viscous effects on the blade boundaries.

Division of the over-all blade-element loss in total pressure into three major categories facilitates discussion of the variation of losses with incidence angle or operating conditions. That is, it is possible to deduce a qualitative loss variation with operating condition based on the assumed flow model and to compare the deduction with measured variations of loss with incidence angle. Such a comparison to a certain degree will indicate whether the flow model is reasonable.

Measured blade-element loss variations. - A typical measured variation of rotor blade-element losses with incidence angles is shown in figure 6(a) for a blade section having supersonic inlet relative Mach numbers. Such loss variations have been observed in tests of several transonic compressors operated at a constant blade speed. Figure 6(b) is similar to figure 6(a) with back pressure as the independent variable.

Note that the solid line in figure 6(a) shows a rise in loss as operation is changed from point B to A (reduction in back pressure) with little change in incidence angle. Point B represents the minimum-loss condition for the solid line. Points A and A' indicate possible loss variations at low back pressures. In some compressors, a reduction in back pressure from point B causes an increase (A) in measured losses with little change in incidence angle, and some data show a reduction in losses (A') at the low back pressures. Since operation of a compressor at either

point A or A' in figure 6(a) is usually not desirable because of low work input and efficiency, point B (operation with back pressure) is generally the maximum-efficiency or the design point, which also is usually near the lowest incidence angle for the blade element. Therefore, the shock configuration for a moderate back pressure (fig. 5(b)) is assumed to be representative of the shock wave at the maximum-efficiency operating condition.

Blade-element loss variations as given by flow model. - With a shock configuration established for maximum-efficiency operation, it is now possible to consider the variation of the three major categories of losses (bow wave, passage shock, and profile losses) with operating condition. A qualitative variation of the three types of losses with back pressure for constant blade speed is shown in figure 7. In addition, the assumed variation in the shock configuration and the corresponding over-all performance characteristics are shown in figure 7.

Bow-wave losses: In reference 16 the losses associated with the bow wave (over the region from point b, c', e, to infinity on fig. 2) were computed as a function of inlet relative Mach number. The magnitude of these losses was small when the required displacement upward from the bow wave to the blade leading edge (shown as h in fig. 2) was small. The displacement h is zero for the case of zero leading-edge thickness and flow entering parallel to the suction surface. It is further noted in reference 16 that the losses of the bow wave are concentrated near the stagnation streamline; 94 to 96 percent of the bow wave losses are located within 4 or 5 times the displacement h from the point b in figure 2.

As shown in figure 7(a), very low bow-wave loss occurs at maximum-efficiency operation (point B), because the incidence angles are usually low and the displacement h of the stagnation streamline is small. Since upstream conditions do not change, the bow-wave loss is constant for low-back-pressure operation (from point A to point B). At higher back pressures (between B and C), the bow-wave losses increase as the back pressure causes the incidence angle and the compression in the bow wave to increase.

Passage shock loss: The passage shock-loss variation with back pressure (fig. 7(b)) can now be considered. The variation of the passage shock loss with reducing back pressures could follow a number of paths (increasing, decreasing, or some combination thereof), depending on the blade shape, solidity, stagger angle, and the three-dimensional aspects of the flow. The envelope of these possible paths is indicated in figure 7(b). If it is presumed that the intersection of the passage shock with the suction surface moves toward the trailing edge for a reduction in back pressure, passage shock losses might increase because the shock occurs at higher Mach numbers. On the other hand, the effect of higher Mach numbers is counteracted by the obliquity of the shock wave. The occurrence of pressure-surface shock waves at low back pressures

(fig. 7(e)) would add to the passage shock losses. In blade elements having high stagger angle and low solidity, the passage shock may move downstream of the trailing edge at low back pressure. Then, if the flow along the pressure surface is wholly supersonic, low passage shock losses could result.

At back pressures greater than at point B, the motion of the passage shock toward the leading edge may cause the shock to occur at lower Mach numbers. Along with this effect is a reduction in inlet relative Mach number (for constant-speed operation). However, the allied increase in incidence angle is in the direction of increasing the Mach number upstream of the passage shock. Therefore, as a best qualitative estimate, the passage shock loss is shown as a constant for back pressures greater than the maximum-efficiency back pressure (point B).

Profile losses: Profile losses (defined as other than shock losses) result from friction forces and the growth of boundary layers associated with the diffusion process on the blade surfaces. For a blade element with supersonic or high subsonic inlet relative Mach numbers, the shock waves contribute importantly to the diffusion process and the boundary-layer growth. As shown for the passage shock losses, there are several possibilities for the variation of profile losses at low back pressures (fig. 7(c)). For the blade-element geometries that allow the passage shock waves to pass downstream of the trailing edge, the profile losses would be low (point A, fig. 6). Blade elements in which shock and boundary-layer interactions occur on both the suction and pressure surfaces may have higher profile losses at low back pressures (point A, fig. 6) than at the maximum-efficiency back pressure (point B).

As back pressure is increased above the value for maximum efficiency, the diffusion downstream of the shock wave (subsonic diffusion) and the profile losses will increase. The variation in profile loss with back pressure shown in figure 7(c) is expected to be much greater than might be observed in low-speed cascades (ref. 19). Poor boundary-layer conditions (high momentum thickness and form factor) downstream of a shock and boundary-layer interaction should result in a large variation in profile loss with changes in the amount of subsonic diffusion.

Over-all blade-element loss: The variations of the three sources of loss with back pressure are qualitatively considered. The sum of these loss factors will be presumed to be the over-all loss as shown in figure 7(d). It should be remembered that this discussion of loss variations is purely qualitative, and shifting the loss variations may change the over-all picture. In addition, some interaction between the loss factors can be expected. Also, the range of back pressure available between choking and unstable operating conditions may be restricted in various rotors. For these reasons, the shape of the over-all loss curve may vary from one rotor to another.

[redacted]

The flow configuration described seems to satisfy the necessary conditions of a flow model. The model is flexible enough to give the variation of operating conditions that have been observed. Qualitatively, the over-all loss variation with operating conditions seems to fit that experimentally observed in transonic compressors (fig. 6). Although the model is complicated, simplifications may be available that allow estimation of the loss level of the various factors involved. The following sections will consider the approximate magnitude of the various loss factors near the condition of maximum-efficiency back pressure (point B, fig. 7).

ESTIMATED SHOCK LOSSES AT MAXIMUM ELEMENT EFFICIENCY

In this preliminary study, the shock losses for the maximum element efficiency of several compressors are computed from a simplified shock configuration, and the results are compared with measured losses. The maximum efficiency is considered because of its importance in establishing design-point performance of a blade row.

Experimental Data

Shock losses were computed for the axial-flow transonic-compressor rotors listed in table I. Table I gives the important rotor geometry and references describing the rotors in detail along with a letter designation for each rotor. For simplicity, only data for double-circular-arc blade sections are included in this analysis, although other types of airfoils could be analyzed by the methods given herein. Blade-element performance data are tabulated in table II for minimum-loss operation (which usually corresponds with maximum element efficiency, point B). The numbers following the rotor-designation letters identify the radial location of the blade-element as a percentage of the passage height from the outer wall. Data points were selected from curves of over-all loss coefficient against incidence angle determined for constant-speed operation of each rotor.

In table II the incidence angles are converted to incidence angles measured relative to the blade suction surface i_s. It can be observed that i_s is slightly negative for these data. According to the previous discussion, this condition of negative incidence should result in low bow-wave losses. Therefore, bow-wave losses can be neglected.

Simplified Shock Model

Since the strength of the passage shock wave varies across the space between the blades, the determination of a shock loss requires an averaging process. If a mass-averaged shock loss is desired, the shape of the

[redacted]

passage shock wave, the Mach number, and the flow angle upstream of the shock are required. For this preliminary study, it is assumed that the average passage shock loss can be approximated by the normal shock loss computed for a Mach number which is the average of the end-point Mach numbers. The one end-point Mach number (at point f in fig. 2) is assumed to be the measured inlet relative Mach number M_1'. The other end-point Mach number (called the peak suction-surface Mach number M_s') is computed, by means of the Prandtl-Meyer expansion equations, from the inlet relative Mach number and the difference between the relative flow angle at the inlet and the angle of a tangent to the suction surface at point f' in figure 2. These assumptions reduce the problem to a determination of the intersection of the passage shock with the suction surface (point f', fig. 2). As shown in figure 8, the point at which the passage shock intersects the suction surface is assumed to be located by a line drawn normal to the midchannel streamline (the mean camber line) from the leading edge of the upper blade. The geometry and equations for locating point f' for double-circular-arc blades are given in appendix B.

Magnitude of Shock Losses

The values of peak suction-surface Mach number, passage shock-loss coefficient, and percent of over-all loss attributed to shocks for the transonic-compressor rotors are given in table II as computed by the method given in the preceding section and appendix B. A quick comparison of percent shock losses for the various rotors can be obtained from figure 9(a), where the ratio of shock-loss coefficient to over-all loss coefficient is plotted against over-all loss coefficient for the tip-section elements (13 percent and less of the passage height from the rotor tip). It is apparent from figure 9(a) that computed shock losses were from 0.2 to over 1.0 of the total losses measured. The few data points for which the computed shock losses are greater than the measured loss are considered later. Most of the rotors considered have between 0.35 and 0.55 of the total loss in the form of shock losses as estimated from the simplified shock model. A similar plot is shown in figure 9(b), in which all midpassage elements are considered (greater than 16 percent of passage height from the outer wall). Even at these radii the shock losses are still high, falling between 0.3 to 1.0 of the total loss.

Whereas early transonic-compressor research indicated that rotors of this type were a simple extension from subsonic compressors, numerous experiments have resulted in losses that could not be correlated by the previously devised methods. To illustrate this point, consider the plot of figure 10(a), where the over-all loss coefficient $\bar{\omega}$ for the measured tip-element data given in table II is plotted against diffusion factor D, a blade-loading parameter (ref. 10). The dotted lines shown represent the loss band given in reference 10. For these transonic-compressor

rotors a large number of data points fall above the loss band, and the diffusion factor D does not seem to be a good method of predicting over-all losses. The previous paragraph indicates that a considerable portion of the over-all loss is in the form of shock losses, which the diffusion factor D would have no way of indicating. It seems reasonable to subtract the computed shock loss from the over-all loss coefficient, the difference being termed the profile loss.

Profile loss is plotted against diffusion factor D in figure 10(b). Profile losses seem to fall more nearly in the band of data given in reference 10. Whereas the diffusion factor D was devised to correlate losses for a given velocity distribution on a compressor blade, it seems to indicate the level of profile losses obtained with the velocity distribution resulting from a shock and subsequent diffusion. The correlation of profile losses is discussed in a later section. Of most importance, however, is the fact that when shock losses are subtracted from the total losses the remainder is in reasonably good agreement with the expected over-all losses without shock; thus, the general magnitude of shock loss computed by this approximate method may be of the proper order.

4056

Similarly, the over-all loss coefficients measured for other than tip elements for these transonic-compressor rotors are plotted against loading parameter in figure 11(a). This figure includes those data available from table II where relative inlet Mach numbers are sonic or greater. Also shown is the typical variation of low-speed-cascade losses with diffusion factor (ref. 10). Again the diffusion factor D does not seem to correlate the magnitude of over-all losses. However, when the shock losses are subtracted from the over-all loss to obtain the estimated profile losses, the data are in better agreement with the low-speed-cascade data, as shown in figure 11(b).

Factors Affecting Shock-Loss Magnitude

It has been shown that shock losses constitute a sizable portion of the over-all losses in a transonic-compressor rotor. Thus far, this report has presented shock losses only for specific cases; however, figure 12 gives a systematic variation of computed shock losses with inlet relative Mach number M_1', peak suction-surface Mach number M_s', and supersonic turning angle (the amount of turning from the upstream flow direction to the intersection of the passage shock wave and the suction surface).

The curves of figure 12 were calculated from the tables of reference 20 by averaging the inlet relative Mach number M_1' and peak suction-surface Mach number M_s' to determine a shock-loss coefficient. In addition, the variables given in figure 12 are independent of a specific

[redacted]

cascade geometry or a blade shape. For the types of transonic compressors generally designed, the inlet relative Mach number is restricted to a smaller range than the peak suction-surface Mach number.

Several examples are given to indicate the use of figure 12. Consider a blade element designed for an inlet relative Mach number of 1.0. An increase in peak suction-surface Mach number from 1.5 to 1.8 causes a threefold increase in shock-loss coefficient. A similar increase in shock-loss coefficient occurs for an increase in inlet relative Mach number from 1.0 to 1.4 when the peak suction-surface Mach number is fixed at 1.5. These examples involve, intrinsically, variations in blade loading, work input, blade shape, and solidity. Therefore, figure 12 does not present the entire process of selecting a compressor design point. It does provide the basis for estimating shock losses in the design of compressors. The effect of shock losses on the efficiency of blade elements can be found using figures 24 and 25 of reference 4 and figure 12 of this report.

Figure 12 shows that, with relative inlet Mach numbers usually considered in transonic compressors (about 1.2) and with surface Mach numbers of 1.7 (as encountered in many of the data used herein), the computed shock-loss coefficient is about 0.1. This shock loss is of the same order of magnitude as the width of the correlation band obtained for the diffusion factor in reference 10. This to some extent explains why references 11 and 13 indicate that, for a surface Mach number of approximately 1.7, losses considerably above the diffusion-factor correlation band could be expected. The curves of figure 12 indicate how shock losses vary at a given relative inlet Mach number and that the shock losses are higher than the normal shock losses at that Mach number. For example, for the relative inlet Mach number of 1.2 the normal-shock-loss coefficient would be relatively low ($\bar{\omega}_S = 0.015$); but, with a peak suction-surface Mach number of 1.7, the computed shock-loss coefficient would be approximately six times that credited to a normal shock at the relative inlet Mach number of 1.2. Thus, inlet relative Mach number is not of itself an indication of the magnitude of the shock losses.

Effect of supersonic turning. - The curves at the top of figure 12 have been constructed to indicate the effect of suction-surface turning in the supersonic region on shock-loss coefficient. These curves show the supersonic turning required to increase the relative inlet Mach number to the suction-surface Mach number indicated. Consider the point of 10° turning with the relative inlet Mach number of 1.0. For this condition the computed shock-loss coefficient would be approximately 0.02. If this 10° of supersonic turning were maintained with the relative inlet Mach number increased to 1.4, the computed shock-loss coefficient would increase approximately seven times. Therefore, blade rows that are expected to operate at these high relative inlet Mach numbers must utilize a much lower suction-surface turning in the supersonic region (forward portion

of the blade) than those operating at low relative inlet Mach numbers; and, even with large decreases in supersonic turning, an increase in shock-loss coefficient must be expected with increasing relative inlet Mach numbers. For the example stated, a decrease in supersonic turning from 10° to 1° must accompany the increase in inlet relative Mach number from 1.0 to 1.4 to maintain a constant shock-loss coefficient.

A low supersonic turning angle can be achieved for double-circular-arc airfoils with low camber angles and thicknesses operating at low incidence angles. If, at high inlet relative Mach numbers, a low camber angle is not feasible because of work-input requirements, blade sections different from the double-circular-arc airfoil must be considered if peak suction-surface Mach numbers and shock losses are to be limited. A desirable airfoil could have a flat suction surface extending from the leading edge to (or nearly to) the expected intersection of the passage shock wave with the suction surface as suggested in reference 17. Whereas such a blade shape would minimize the shock losses, the effect on profile losses is unknown.

Effect of solidity. - Suction-surface turning angle in the supersonic region is influenced by blade camber, thickness, stagger angle, and solidity for a certain airfoil type. As an illustration of the effect of solidity, the rotor of reference 13 (double-circular-arc airfoils) indicated a suction-surface turning in the supersonic region (as calculated by the simplified shock model) of approximately 11° at a solidity of 1.04. As the solidity was decreased to approximately 0.88 with the blade camber remaining the same, the suction-surface turning angle was increased to approximately 14°. As the solidity was further decreased to 0.66, the suction-surface turning in the supersonic region was about 19°. These points are indicated in figure 12. Experimental data were obtained for all three solidities at a relative inlet Mach number of approximately 1.1. The curves of figure 12 indicate that the computed shock-loss coefficients are approximately 0.055, 0.075, and about 0.120 for the solidities 1.04, 0.88, and 0.66, respectively. This is indicative of the measured variations of losses with solidity that were obtained in the rotor tests (ref. 13).

Three-dimensional effects. - An indication of possible three-dimensional effects on passage shock losses may be deduced from the data in table II. Four different rotors (H, I, N, and Q) have a contoured tip over the rotor. (Rotors R and S are lower-solidity versions of Q). Of these, the rotors N and Q have measured total losses less than the passage shock losses computed by the methods of this report. By contouring the rotor tip, some three-dimensional compression (reduction in streamline spacing) of the supersonic flow can be obtained, resulting in a lower local Mach number than that obtained in the simplified two-dimensional solution. If the flow entering the rotor is compressed in this manner, a two-dimensional solution could overestimate the surface

Mach number M_s' and passage shock-loss coefficient. In this report, comparison of rotors M and N is particularly graphic. Both rotors are identical except that rotor M has a constant-radius tip and rotor N has a contoured tip. As reported in reference 21, which presents the comparative results of testing rotors M and N, the reduction in tip-region losses accompanying the contouring of the tip could not be accounted for solely on the basis of a reduction in blade loading. It can be speculated that contouring the tip of rotor N reduced the shock losses. The fact that the computed shock losses for some rotors with contoured tips (H and J) did not exceed the measured total losses does not necessarily invalidate the idea that a tip contour can be used to reduce shock. However, it may be concluded that, to be effective, the tip contour must be properly shaped.

PROFILE LOSSES

The previous discussion has dealt with factors affecting shock losses and an approximate magnitude of shock losses. It was assumed that the over-all losses in a compressor blade element could be divided into three main parts at the maximum-efficiency point: (1) bow-wave losses, which were considered negligible, (2) passage shock losses, which in effect are a free-stream loss, and (3) losses related to the blade profile.

Interaction of Shock and Boundary Layer

The profile losses have usually been considered to be related to the boundary-layer growth on the suction surface of the blade. This growth of boundary layer may be due to the adverse pressure gradients through normal diffusion or the interaction of the shock and boundary layer. The previous section has shown that the flow Mach number at the shock may be high. At these high Mach numbers boundary-layer separation at the shock may be inevitable, as indicated by references 22 and 23. The conditions of the boundary layer upstream of the shock are not known. If the shock is moved well forward, it is possible that the boundary layer remains laminar to the shock; whereas, if the shock is well back on the blade, it is possible that the boundary layer is turbulent. With either type of boundary layer, however, the pressure rise due to the shock is felt forward of the shock in the boundary layer. With a laminar boundary layer, the pressure rise is felt a considerable distance forward; the boundary layer thickens and the mainstream is deflected away from the blade surface, resulting in the compression waves shown in figure 13(a). These compression waves coalesce into a normal shock some distance away from the suction surface. It is interesting to note that the loss in total pressure over this series of compression waves may be less than the corresponding compression over a normal shock. A similar flow

pattern is observed if the boundary layer is turbulent. However, in this case the static-pressure rise is not felt as far forward. Compression waves are also noted outside the turbulent boundary layer, but they exist in a smaller region.

Of most concern must be the fact that, for either type of boundary layer, flow separation probably exists near the shock plane. Thus, the factors affecting this flow separation must be considered. Once the mainstream flow leaves the suction surface, two effects are available to limit the amount of separation. First, the pressure surface of the upper blade will cause the stream to turn toward the suction surface and limit the extent of the separation. Secondly, local conditions of choking may limit the magnitude of flow separations. Thus, the size of the separated region would not grow without limit. It is possible that, under some condition of low back pressure, the flow may reattach to the blade surface, resulting in local expansions and compressions as shown in figure 13(b), or the flow may continue separated throughout the blade row. Thus, the flow model cannot explicitly be defined for the flow in this region at the present time.

4556

Suction-Surface Velocity Variations

The flow model for transonic-compressor blade elements indicates that the boundary layer on the suction surface is the major contributor to the profile losses for operation at maximum-efficiency and higher back-pressure conditions. As an extension of the previous discussions, it is possible to deduce a typical velocity variation along the suction surface of transonic blade elements. In addition, the origin of profile losses can be considered in detail.

For convenience, the flow along the suction surface can be divided into three regions as shown in figure 14. In the first region, near the leading edge of the blades, the velocity outside the suction-surface boundary layer is supersonic, and the flow is accelerating. In spite of the high velocities, the profile loss generated in this region is probably small because of the favorable velocity gradient. There is the possibility (depending on the free-stream turbulence) that the suction-surface boundary layer is laminar in this region, because the accelerating flow field tends to maintain a laminar layer.

In the second region, the velocity variations are influenced largely by the shock configuration. A short distance upstream of the shock, the boundary layer senses the pressure increase imposed by the shock, and a large decrease in the suction-surface velocity occurs in the region of the shock system (fig. 14). The boundary-layer growth through the entire shock system (region 2) is very rapid and contributes sizably to the profile losses. Since the peak suction-surface Mach numbers were

computed to be 1.5 or greater for most of the blade elements examined, separation of the boundary layer at the shock is almost inevitable (ref. 22).

In the third region, which is downstream of the shock system, a subsonic diffusion generally occurs. In some cases there might be local expansion above Mach 1.0 and subsequent compression shocks at the point of reattachment followed by subsonic diffusion. In other cases, the subsonic diffusion may be from Mach 1.0 directly to the discharge velocity. In either case the boundary layer at the beginning of region 3 is in a very poor condition to sustain further diffusion, in that it either has been or is in a separated condition, and the continual adverse pressure gradient may be expected to cause sizable losses. The relative magnitude of these losses as compared with those of the second region is further obscured by the fact that no published experimental data are available for the profile loss encountered in the case of boundary-layer - shock interaction in a field similar to that described.

The velocity profile over the blade suction surface is shown schematically in figure 15(a) for the type of flow described. The suction-surface velocity in the first region is increasing rapidly to some rather high value at point B. In the second region, the suction-surface velocity drops rapidly; this is the effect of the shock and the shock - boundary-layer interaction. At point C, the velocity is approximately sonic. Then, if local expansion occurs (fig. 15(a)), the velocity increases slightly to point D, and a compression shock follows to the end of region 2 at D'. The suction-surface velocity then continues to decrease by subsonic diffusion to point E at the trailing edge of the blade. The other case (i.e., without local reexpansion above sonic velocity) is shown schematically in figure 15(b). In this case the velocity decreases in the region of the shock to near sonic velocity, remains nearly constant for a short distance, and then drops off again in the subsonic diffusion region.

The velocity profiles discussed are in contrast to the velocity profile usually encountered at low relative inlet Mach numbers, for which the suction-surface velocity increases very rapidly to some high value near the leading edge and then drops off gradually to the discharge value at the trailing edge of the blade (fig. 15(c)). Some success in correlating losses in the latter case has been obtained by presuming that the losses were related to the ratio of the maximum suction-surface velocity to the discharge velocity. Such a correlating ratio probably worked reasonably well because the profile losses were encountered mainly in this gradual diffusion from the maximum to the discharge velocity, and the initial state of the boundary layer does not vary greatly (ref. 1). At high Mach numbers, there can be several regions in which profile losses are generated, and it may be that a simple velocity ratio cannot be expected to correlate the profile losses. That is, the losses of region 2 (fig. 14) may be related to some velocity ratio or correlating parameter

and those of region 3 to some other correlating parameter. In addition, the boundary-layer conditions at the start of the diffusion process may vary considerably with cascade geometry for flows with shock waves. For this reason, too, a simple velocity ratio may not describe accurately the boundary-layer growth and profile losses for transonic blade elements.

Study of Suction-Surface Diffusion Parameters

In this preliminary analysis the profile loss has been defined as the difference between the measured over-all loss and the estimated shock loss. This profile loss is plotted against the diffusion factor D in figures 10(b) and 11(b); and, since the data fall generally within the range of previous experience, it is presumed that estimation of shock losses was reasonably good. However, the flow conditions are very different from those of the flow model for which the diffusion factor was established. As a natural extension of the computations of peak suction-surface Mach numbers M_s', it is possible to compute other suction-surface diffusion parameters. Several of the parameters will be considered in correlating profile losses.

The estimated profile losses for the blade-element data shown in table II are plotted against the ratio of calculated peak suction-surface velocity to discharge relative velocity in figure 16. The data for the tip region are given in figure 16(a) and for midpassage in figure 16(b). The profile loss seems to increase as greater ratios of velocity are obtained for the tip-region data. The spread of the losses obtained is similar to that obtained for the diffusion factor D. At the other radial positions the data do not indicate any particular trend of profile losses with this ratio of velocities over the range of data available for maximum-efficiency loss. This, too, is similar to the plot of profile loss against diffusion factor for midpassage elements.

Another parameter based on computed peak velocity and the measured discharge conditions is the static-pressure-rise coefficient $(p_2 - p_s)/(P_1' - p_s)$. The computed profile losses are plotted against the static-pressure-rise coefficient in figure 17, and no particular trends are evident. These diffusion parameters depend on the estimated peak velocity on the blade suction surface. Also, an estimated shock loss subtracted from a total loss containing some experimental inaccuracies was used to determine a profile loss. Thus, the lack of correlation (V_s/V_2' and $(p_2 - p_s)/(P_1' - p_s)$) in this preliminary analysis should not completely discredit these fundamental parameters.

The above-mentioned parameters, which were taken to be indicative of the diffusion along the blade suction surface, describe the total diffusion from estimated peak velocity to the discharge velocity. The idea

has been advanced that the flow velocity just behind the point of separation may be near sonic. Thus, the subsonic diffusion would be from approximately a Mach number of 1.0 to the discharge conditions. The velocity ratio for Mach number of 1.0 to discharge relative velocity has been computed for these data and is plotted against the estimated profile loss in figure 18. No particular trend in profile loss is obtained, possibly as a result of the necessary approximations and the fact that this particular ratio of velocities is only a part of the over-all diffusion along the suction surface. It is of interest to note that a major portion of the velocity change is obtained in the region of the shock. The range of the ratio of peak velocity to discharge velocity V_s/V_2' is about 1.4 to 2.5 (fig. 16), whereas the ratio of sonic velocity to discharge velocity is from about 0.9 to 1.6 (fig. 18). Thus, the change in velocity obtained in the subsonic diffusion region is relatively small for all the data used in this study.

4336

In summary, several parameters (including the diffusion factor D) that are related to the suction-surface velocity variations have been considered for correlating profile losses. The velocity ratio for the subsonic portion of the diffusion process and the static-pressure-rise coefficient do not afford a basis for correlating profile losses. The profile losses varied with diffusion factor D and the ratio of maximum to outlet velocity V_s/V_2' in essentially the same manner. Several explanations for these observations can be given. All the parameters are based on the hypothesis that there is at least a first-order dependence of profile losses on suction-surface diffusion. Particularly in the presence of shock waves, other factors (shock and boundary-layer interactions, initial condition of the boundary layer, blade shape) may be as important as the diffusion. In addition, the profile loss is approximate because of the errors encountered in measuring over-all losses and because the shock losses were obtained by an approximate method. The values of the diffusion parameters themselves depend on an estimate of such terms as the peak velocities determined from two-dimensional solutions. Furthermore, it is recognized that the data selected may not correspond to the condition for minimum profile losses. Thus, for a study of the profile losses it may be better to use the data obtained over a range of operating conditions rather than the maximum-element-efficiency data. However, at present there is no simplified method for estimating shock-loss variation over a range of operating conditions.

CO-3 back

CONCLUDING REMARKS

The following summation can be made from the preliminary study of losses of supersonic blade elements of transonic-compressor rotors:

[redacted]

1. The shock configuration existing in transonic-compressor rotors consists of a bow wave and a passage shock, the shape and location of the shock waves depending on the operating conditions.

2. A simple model of this shock configuration was used to estimate passage shock losses at maximum element efficiency. The losses associated with the passage shock generally vary from 0.35 to 0.55 of the over-all measured losses for the transonic compressors considered.

3. A reasonable approximation of the passage shock loss can be obtained from the average of the peak suction-surface Mach number upstream of the shock and the relative inlet Mach number. Prandtl-Meyer expansion equations were used to compute the peak suction-surface Mach number.

4. In many cases computed suction-surface Mach numbers were high for the double-circular-arc airfoils considered. Therefore, in many of the transonic compressors tested to date, a separation of the suction-surface boundary layer undoubtedly occurred as a result of the interaction between the shock and boundary layer.

5. Profile losses, which are defined as the over-all measured loss minus the computed shock loss, are of about the same order of magnitude as obtained in investigations in which shock losses were not encountered.

6. Several flow parameters indicative of the magnitude of diffusion on the blade suction surface were considered. However, no consistent variation of profile loss was obtained with these parameters. Whereas the diffusion factor D is not entirely adequate for the flow model with shocks, the profile losses for the transonic-compressor data used in this study fall reasonably well within the loss band previously obtained for subsonic-compressor rotors.

Lewis Flight Propulsion Laboratory
National Advisory Committee for Aeronautics
Cleveland, Ohio, January 31, 1957

APPENDIX A

SYMBOLS

c	blade chord, in.
D	diffusion factor (ref. 10)
h	height of streamline deflection from bow wave to blade leading edge
i	incidence angle, angle between relative inlet-air direction and tangent to blade mean camber line at leading edge, deg
i_s	incidence angle, angle between relative inlet-air direction and tangent to suction surface of blade leading edge, deg
M_s'	peak suction-surface Mach number
M_1'	relative inlet Mach number
P	total pressure, lb/sq ft
p	static pressure, lb/sq ft
p_s	static pressure at peak suction-surface Mach number, lb/sq ft
q	dynamic pressure
R_m	radius of curvature of mean camber line, in.
R_s	radius of curvature of blade suction surface, in.
r_{le}	blade leading-edge radius, in.
s	blade spacing, in.
t	blade thickness, in.
U_t	rotor tip speed, ft/sec
V	air velocity, ft/sec
β	air angle, angle between air velocity and axial direction, deg
γ^o	blade-chord angle, angle between blade chord and axial direction, deg

η_{ad} adiabatic efficiency

θ ratio of temperature to NACA standard sea-level temperature

$\varkappa$ blade angle, angle between tangent to blade mean camber line and axial direction, deg

ν Prandtl-Meyer expansion angle (ref. 20)

ξ_c angle between tangent to blade suction surface at peak Mach number point and chord, deg

ξ_z angle between tangent to blade suction surface at peak Mach number point and axial direction, deg

Σ angle used in fig. 20, deg

σ blade solidity, ratio of chord to spacing

φ camber angle, $\varkappa_1 - \varkappa_2$, deg

$\bar{\omega}$ total-pressure-loss coefficient, over-all-measured loss

$\bar{\omega}_s$ total-pressure-loss coefficient, calculated shock loss

Subscripts:

a upstream of passage shock

b downstream of passage shock

id ideal

max maximum

s suction surface

0 at Mach number 1.0

1 rotor inlet

2 rotor outlet

Superscripts:

' relative to rotor

– mass-averaged value

APPENDIX B

CALCULATION OF PASSAGE SHOCK LOSSES

Figure 19, which presents the geometry of double-circular-arc airfoils, illustrates the principles involved in computing the peak suction-surface Mach number M_s' for any blade section of known geometry. The information necessary for the calculation is the inlet relative Mach number M_1', the inlet relative air direction β_1', and the point f' at which the passage shock wave intersects the suction surface. With point f' known, the flow direction (equivalent to the suction-surface direction ξ_z) at this point can be found from the blade geometry or coordinates. Then, the calculation of peak suction-surface Mach number involves the use of the tables of reference 20, which give values of the Prandtl-Meyer expansion angle ν as a function of Mach number. The method is as follows:

(1) Determine ν_1', the Prandtl-Meyer expansion angle for the inlet relative Mach number M_1'. (This step restricts the method to blade elements with an inlet relative Mach number greater than or equal to 1.0.)

(2) Compute the amount of supersonic turning $\Delta\nu$, which is defined as $\beta_1' - \xi_z$.

(3) Find the Prandtl-Meyer angle for the flow at the passage shock wave (point f'):

$$\nu_s' = \nu_1' + \Delta\nu = \nu_1' + \beta_1' - \xi_z \tag{B1}$$

(4) The peak suction-surface Mach number M_s' is the Mach number in the tables (ref. 20) which corresponds to ν_s'.

The shock-loss coefficient is computed from

$$\bar{\omega}_s = \frac{1 - \left(\frac{P_b'}{P_a'}\right)}{1 - \frac{P_1}{P_1'}} \tag{B2}$$

where (P_b'/P_a') is the normal-shock recovery factor determined for a Mach number equal to the average of the peak suction-surface Mach number M_s' and the inlet relative Mach number M_1'.

For double-circular-arc airfoils, the suction-surface direction ξ_z can be found from the distance x (fig. 19), which is the distance between the shock intersection and the center of the leading-edge radius. According to figure 19,

$$\xi_c = \arcsin\left[\sin\frac{\varphi_s}{2}\left(\frac{x}{c'/2} - 1\right)\right] \tag{B3}$$

where

$$c' = c - 2r_{le}$$

and

$$\frac{\varphi_s}{2} = 2 \arctan\left(\frac{1 - \cos\frac{\varphi}{2}}{\sin\frac{\varphi}{2}} + \frac{t_{max}}{c'} - \frac{2r_{le}}{c'}\right)$$

Then,

$$\xi_z = \gamma^o - \xi_c$$

and equation (B1) becomes

$$\nu_s' = \nu_1' + \beta_1' - (\gamma^o - \xi_c) \tag{B4}$$

Now, with $\gamma^o = \varkappa_1 - \frac{\varphi}{2}$ and $i = \beta_1' - \varkappa_1$,

$$\nu_s' = \nu_1' + i + \frac{\varphi}{2} + \xi_c \tag{B5}$$

The location of the intersection of the passage shock with the suction surface (point f') is not known for the rotor data considered herein. Consequently, an assumption is required. Point f' was located for double-circular-arc airfoils by the construction shown in figure 20. The straight line which intersects the suction surface at point f' passes through the leading edge of the adjacent blade and is normal to the midchannel streamline. The midchannel streamline is assumed to be a blade mean camber line positioned midway between two blades. As shown in figure 20, these assumptions lead to the following equation for the distance x:

$$\frac{x}{c'/2} = 1 + \sin 2\Sigma \cot \frac{\varphi}{2} - \cos 2\Sigma \qquad \text{(B6)}$$

where

$$\Sigma = \arctan\left(\frac{\sin \varkappa_1 \sin \frac{\varphi}{2}}{\sigma' + \cos \varkappa_1 \sin \frac{\varphi}{2}}\right)$$

and

$$\sigma' = \frac{c'}{s} = \sigma\left(1 - \frac{2r_{le}}{c}\right)$$

Thus, $\frac{x}{c'/2}$ can be determined from equation (B6), and with equations (B3) and (B5) the Prandtl-Meyer expansion angle ν_s' for the peak suction-surface Mach number M_s' can be found.

The location of point f' by this method is arbitrary; however, the approach gives a systematic study of shock losses in the compressors considered in this report. Two other systematic definitions of the shock location were included in this study. One definition was based on a line drawn perpendicular to the chord line; the other method located point f' along a line of minimum distance between two adjacent blades. The shock losses determined from each of these definitions were not substantially different from the ones reported herein.

REFERENCES

1. Creagh, John W. R.: Performance Characteristics of an Axial-Flow Transonic Compressor Operating up to Tip Relative Inlet Mach Numbers of 1.34. NACA RM E56D27, 1956.

2. Hatch, James E., Giamati, Charles C., and Jackson, Robert J.: Application of Radial-Equilibrium Condition to Axial-Flow Turbomachine Design Including Consideration of Change of Entropy with Radius Downstream of Blade Row. NACA RM E54A20, 1954.

3. Lieblein, Seymour: Review of High-Performance Axial-Flow-Compressor Blade-Element Theory. NACA RM E53L22, 1954.

4. Robbins, William H., Jackson, Robert J., and Lieblein, Seymour: Blade-Element Flow in Annular Cascades. Ch. VII of Aerodynamic Design of Axial-Flow Compressors, vol. II. NACA RM E56B03a, 1956, pp. 97-156.

5. Schwenk, Francis C., Lieblein, Seymour, and Lewis, George W., Jr.: Experimental Investigation of an Axial-Flow Compressor Inlet Stage Operating at Transonic Relative Inlet Mach Numbers. III - Blade-Row Performance of Stage with Transonic Rotor and Subsonic Stator at Corrected Tip Speeds of 800 and 1000 Feet Per Second. NACA RM E53G17, 1953.

6. Sandercock, Donald M., Lieblein, Seymour, and Schwenk, Francis C.: Experimental Investigation of an Axial-Flow Compressor Inlet Stage Operating at Transonic Relative Inlet Mach Numbers. IV - Stage and Blade-Row Performance of Stage with Axial-Discharge Stators. NACA RM E54C26, 1954.

7. Lewis, George W., Jr., and Schwenk, Francis C.: Experimental Investigation of a Transonic Axial-Flow-Compressor Rotor with Double-Circular-Arc Airfoil Blade Sections. II - Blade-Element Performance. NACA RM E54J08, 1955.

8. Schwenk, Francis C., and Tysl, Edward R.: Experimental Investigation of a Transonic Compressor Rotor with a 1.5-Inch Chord Length and an Aspect Ratio of 3.0. II - Blade-Element Performance. NACA RM E55F10, 1955.

9. Montgomery, John C., and Glaser, Frederick W.: Experimental Investigation of a 0.4 Hub-Tip Diameter Ratio Axial-Flow Compressor Inlet Stage at Transonic Inlet Relative Mach Numbers. II - Stage and Blade-Element Performance. NACA RM E54I29, 1955.

10. Lieblein, Seymour, Schwenk, Francis C., and Broderick, Robert L.: Diffusion Factor for Estimating Losses and Limiting Blade Loadings in Axial-Flow-Compressor Blade Elements. NACA RM E53D01, 1953.

11. Schwenk, Francis C., Lewis, George W., Jr., and Lieblein, Seymour: Experimental Investigation of an Axial-Flow-Compressor Inlet Stage Operating at Transonic Relative Inlet Mach Numbers. V - Rotor Blade-Element Performance at a Reduced Blade Angle. NACA RM E56J17, 1957.

12. Wright, Linwood C., and Wilcox, Ward W.: Investigation of Two-Stage Counterrotating Compressor. II - First-Rotor Blade-Element Performance. NACA RM E56G09, 1956.

13. Schwenk, Francis C., and Lewis, George W., Jr.: Experimental Investigation of a Transonic Axial-Flow-Compressor Rotor with Double-Circular-Arc Blade Sections. III - Comparison of Blade-Element Performance with Three Levels of Solidity. NACA RM E55F01, 1955.

14. Tysl, Edward R., and Schwenk, Francis C.: Experimental Investigation of a Transonic Compressor Rotor with a 1.5-Inch Chord Length and an Aspect Ratio of 3.0. III - Blade-Element and Over-All Performance at Three Solidity Levels. NACA RM E56D06, 1956.

15. Fessler, Theodore E., and Hartmann, Melvin J.: Preliminary Survey of Compressor Rotor-Blade Wakes and Other Flow Phenomena with a Hot-Wire Anemometer. NACA RM E56A13, 1956.

16. Graham, Robert C., Klapproth, John F., and Barina, Frank J.: Investigation of Off-Design Performance of Shock-in-Rotor Type Supersonic Blading. NACA RM E51C22, 1951.

17. Staniforth, R.: A Note on Compressor Operation at Transonic Relative Inlet Mach Numbers. Memo. No. M.224, British N.G.T.E., July 1954.

18. Kantrowitz, Arthur: The Supersonic Axial-Flow Compressor. NACA Rep. 974, 1950. (Supersedes NACA ACR L6D02.)

19. Lieblein, Seymour: Analysis of Experimental Low-Speed Loss and Stall Characteristics of Two-Dimensional Compressor Blade Cascades. NACA RM E57A28, 1957.

20. Ames Research Staff: Equations, Tables, and Charts for Compressible Flow. NACA Rep. 1135, 1953. (Supersedes NACA TN 1428.)

21. Montgomery, John C., and Glaser, Frederick: Experimental Investigation of a 0.4 Hub-Tip Diameter Ratio Axial-Flow Compressor Inlet Stage at Transonic Inlet Relative Mach Numbers. III - Effect of Tip Taper on Over-All and Blade-Element Performances. NACA RM E55L09, 1956.

22. Bogdonoff, Seymour M.: Axial Flow Compressors. Pt. I - A Study of the Fluid Mechanics Problems Associated with Optimizing Performance. WADC Tech. Rep. TR 54-514, Wright Air Dev. Center, Wright-Patterson Air Force Base, Oct. 1954. (Contract AF-33(038)-18190.)

23. Nussdorfer, T. J.: Some Observations of Shock-Induced Turbulent Separation on Supersonic Diffusers. NACA RM E51L26, 1954.

24. Robbins, William H., and Glaser, Frederick W.: Investigation of an Axial-Flow-Compressor Rotor with Circular-Arc Blades Operating up to a Rotor-Inlet Relative Mach Number of 1.22. NACA RM E53D24, 1953.

25. Sandercock, Donald M., and Kovach, Karl: Experimental Investigation of a Five-Stage Axial-Flow Research Compressor with Transonic Rotors in All Stages. III - Interstage Data and Individual Stage Performance Characteristics. NACA RM E56G24, 1956.

[redacted]

TABLE I. - DETAILS OF ROTORS

Rotor	Reference	Tip radius, in.		Hub-tip radius ratio		Leading-edge radius, r_{le}, in.	Number of blades	Tip design speed, $U_t/\sqrt{\theta}$, ft/sec	Blade-element position, passage from outer wall, percent	Chord, c, in.	Solidity, σ	Camber angle, Φ, deg	Chord angle, γ^o, deg	Maximum thickness to chord ratio, t_{max}/c
		Inlet	Outlet	Inlet	Outlet									
A	7 and 13	7.0	7.0	0.50	0.572	0.015	19	1000	13 18	2.27 2.25	1.04 1.06	13.8 14.6	44.1 42.9	0.05 .05
B	13	7.0	7.0	0.50	0.572	0.015	16	1000	13 18	2.27 2.25	0.88 .89	13.8 14.6	44.1 42.9	0.05 .05
C	13	7.0	7.0	0.50	0.572	0.015	12	1000	13 18	2.27 2.25	0.66 .67	13.8 14.6	44.1 42.9	0.05 .05
D	24	7.0	7.0	0.491	0.536	0.010	23	1120	10	1.50	0.826	4.3	51.95	0.05
E	5 and 6	8.68	8.68	0.525	0.60	0.015	21	1000	11 17	3.18 3.17	1.29 1.32	22.1 22.6	43.15 42.25	0.048 .050
F	11	8.68	8.68	0.525	0.60	0.015	21	1000	11 17	3.18 3.17	1.29 1.32	22.1 22.6	37.15 36.25	0.048 .050
H	1	8.0	7.75	0.500	0.593	0.010	27	1300	11 18 50	1.75 ↓	1.006 1.038 1.233	11.3 10.7 10.4	52.2 50.95 43.8	0.053 .055 .064
I	12	8.0	7.6	0.500	0.611	0.015	22	1260	10 20 40 50 60	2.75 ↓	1.282 1.332 1.443 ~~~~ 1.591	28.22 31.84 36.21 38.45 41.00	41.48 39.73 35.85 32.93 24.78	0.049 .053 .060 .065 .069
J	8 and 14	9.0	9.0	0.500	0.556	0.010	35	1000	10 16	1.50 1.50	1.00 1.03	6.0 7.0	47.6 46.3	0.061 .063
K	14	9.0	9.0	0.500	0.556	0.010	28	1000	10 16	1.50 1.50	0.80 .82	6.0 7.0	47.6 46.3	0.061 .063
L	14	9.0	9.0	0.500	0.556	0.010	22	1000	10 16	1.50 1.50	0.63 .65	6.0 7.0	47.6 46.3	0.061 .063
M	9	7.0	7.0	0.400	0.522	0.010	20	1000	10	2.00	0.963	11.4	46.7	0.053
N	21	7.0	6.75	0.400	0.552	0.010	20	1000	10	2.00	0.978	14.6	45.6	0.053
O	25	10.0	10.0	0.50	0.57	0.015	23	1100	16 25 33	2.67 ↓	1.048 1.092 1.136	12.7 13.9 15.6	46.95 45.05 43.00	0.054 .055 .057
P	25	10.0	10.0	0.62	0.675	0.015	27	1100	16 25 33 50	2.73 ↓	1.232 1.263 1.304 1.379	16.5 17.9 19.5 23.6	45.55 45.95 42.15 38.10	0.054 .055 .057 .062
Q	15	10.0	9.55	0.60	0.628	0.015	21	1000	9	2.71	0.972	17.4	46.88	0.074
R	15	10.0	9.55	0.60	0.628	0.015	15	1000	9	2.71	0.833	17.4	46.88	0.074
S	15	10.0	9.55	0.60	0.628	0.015	18	1000	9	2.71	0.694	17.4	46.88	0.074

[redacted]

4336

TABLE II. - SUMMARY DATA FOR TRANSONIC ROTORS

Rotor	Inlet relative Mach number, M_1'	Total-pressure ratio, P_2/P_1	Adiabatic efficiency, η_{ad}	Measured loss coefficient, ω	Diffusion factor, D	Incidence angle, deg		Suction-surface Mach number, M_s'	Shock-loss coefficient, ω_s	Loss ratio, ω_s/ω	Profile loss, $\omega - \omega_s$	$\left(\frac{\Delta p}{q}\right)_{M_s}$	V_s/V_1'	V_0/V_1'	Data-point symbol
						i	i_s								
A-13	1.081	1.417	0.803	0.149	0.406	2.74	-1.50	1.607	0.056	0.376	0.093	0.561	1.903	1.329	◇
	1.070	1.461	.822	.145	.514	3.38	-.86	1.622	.057	.393	.088	.595	2.03	1.401	
	1.067	1.459	.806	.161	.507	3.60	-.64	1.628	.058	.360	.103	.600	2.03	1.400	
A-18	1.060	1.426	0.848	0.114	0.456	2.83	-1.41	1.601	0.052	0.456	0.062	0.578	1.893	1.221	◆
	1.049	1.469	.867	.107	.497	3.51	-.73	1.618	.054	.500	.054	.617	2.000	1.230	
	1.045	1.467	.856	.117	.486	3.73	-.51	1.624	.054	.462	.063	.617	1.950	1.324	
B-13	1.093	1.343	0.734	0.182	0.407	1.90	-2.34	1.678	0.072	0.396	0.110	0.527	1.795	1.106	▽
	1.083	1.344	.744	.174	.409	2.01	-2.23	1.680	.073	.420	.101	.536	1.810	1.156	
	1.081	1.378	.759	.193	.476	2.62	-1.62	1.693	.074	.383	.119	.579	1.945	1.223	
B-18	1.074	1.356	0.788	0.144	0.404	1.93	-2.31	1.688	0.067	0.465	0.077	0.539	1.790	1.329	▼
	1.073	1.360	.795	.141	.407	2.09	-2.15	1.671	.068	.482	.073	.552	1.815	1.394	
	1.059	1.403	.817	.136	.461	2.74	-1.50	1.686	.070	.515	.066	.596	1.915	1.385	
C-13	1.107	1.212	0.599	0.217	0.334	1.30	-2.94	1.852	0.119	0.548	0.098	0.474	1.728	1.222	◇
	1.101	1.251	.632	.218	.379	1.58	-2.66	1.858	.120	.550	.098	.510	1.805	1.239	
	1.089	1.293	.666	.219	.445	2.22	-2.02	1.872	.122	.557	.097	.517	1.931	1.301	
C-18	1.087	1.218	0.820	0.207	0.355	1.57	-2.87	1.856	0.112	0.541	0.095	0.485	1.743	1.122	◆
	1.081	1.262	.673	.196	.381	1.63	-2.61	1.839	.111	.566	.085	.525	1.815	1.169	
	1.066	1.305	.716	.186	.452	2.30	-1.94	1.855	.114	.613	.072	.565	1.941	1.242	
D-10	1.202	———	0.675	0.170	0.330	1.70	-2.56	1.553	0.062	0.365	0.108	0.386	1.510	1.081	○
	1.171	———	.720	.196	.477	3.51	-.75	1.589	.065	.332	.131	.477	1.720	1.213	
	1.148	———	.668	.252	.516	4.71	.45	1.611	.066	.284	.186	.495	1.884	1.315	
	1.077	———	.779	.109	.325	.87	-3.39	1.433	.026	.259	.083	.450	1.555	1.174	
	1.081	———	.795	.121	.358	1.86	-2.40	1.458	.028	.251	.093	.500	1.605	1.223	
	1.040	———	.768	.144	.388	3.39	-.87	1.499	.032	.222	.112	.528	1.730	1.269	
E-11	1.170	1.608	0.852	0.125	0.481	1.8	-2.61	1.710	0.092	0.736	0.033	0.551	1.920	1.291	◁
	1.153	1.673	.828	.166	.498	2.2	-2.21	1.710	.089	.536	.077	.602	2.00	1.345	
	1.148	1.719	.842	.159	.520	2.61	-1.80	1.718	.090	.566	.069	.624	2.06	1.381	
	1.038	1.563	.861	.111	.482	3.10	-1.31	1.666	.062	.559	.049	.854	2.29	1.429	
	1.056	1.555	.884	.105	.482	1.80	-2.61	1.633	.058	.552	.047	.640	2.04	1.414	
	1.018	1.564	.850	.145	.522	4.00	-.41	1.692	.065	.448	.080	.674	2.235	1.516	
E-17	1.145	1.633	0.909	0.080	0.444	2.00	-2.62	1.667	0.082	1.025	-0.002	0.565	1.762	1.257	△
	1.128	1.677	.892	.102	.476	2.60	-2.02	1.695	.081	.794	.021	.622	1.970	1.331	
	1.120	1.725	.905	.094	.500	2.95	-1.67	1.702	.082	.872	.012	.642	2.051	1.383	
	1.013	1.561	.922	.072	.460	3.40	-1.22	1.660	.058	.806	.014	.669	2.037	1.396	
	1.033	1.550	.913	.078	.452	2.10	-2.52	1.625	.052	.667	.026	.660	2.117	1.472	
F-11	1.216	1.526	0.611	0.357	0.616	5.2	0.79	1.810	0.125	0.350	0.232	0.558	2.35	1.527	▽
	1.206	1.556	.616	.366	.647	5.5	1.09	1.811	.124	.339	.242	.575	2.47	1.602	
	1.192	1.587	.644	.345	.654	6.0	1.59	1.817	.125	.357	.222	.581	2.495	1.615	
	1.197	1.604	.644	.350	.664	6.1	1.69	1.825	.126	.360	.224	.585	2.53	1.636	
	1.128	1.522	.748	.215	.545	3.6	-.81	1.684	.079	.367	.136	.576	2.155	1.463	
	1.117	1.533	.745	.225	.566	4.1	-.31	1.693	.079	.351	.146	.628	2.24	1.516	
	1.108	1.545	.737	.239	.587	4.6	.19	1.704	.081	.339	.158	.655	2.32	1.563	
	1.092	1.554	.721	.268	.632	5.8	1.39	1.735	.086	.323	.180	.647	2.51	1.675	
F-17	1.190	1.584	0.699	0.278	0.562	5.26	0.64	1.827	0.125	0.453	0.151	0.577	2.212	1.426	▷
	1.180	1.625	.713	.275	.585	5.49	.87	1.827	.124	.454	.149	.592	2.280	1.470	
	1.166	1.626	.721	.267	.591	6.02	1.40	1.834	.124	.464	.143	.601	2.313	1.489	
	1.170	1.639	.712	.280	.600	6.18	1.56	1.843	.127	.454	.153	.607	2.348	1.506	
	1.104	1.551	.833	.138	.504	3.60	-1.02	1.705	.081	.587	.057	.617	2.081	1.402	
	1.092	1.558	.829	.146	.526	4.21	-.41	1.718	.082	.562	.064	.649	2.170	1.454	
	1.084	1.562	.816	.162	.538	4.66	.04	1.728	.083	.512	.078	.657	2.260	1.509	
	1.074	1.562	.815	.164	.558	5.20	.58	1.741	.084	.512	.080	.658	2.302	1.529	
H-11	1.282	1.320	0.744	0.163	0.343	3.7	-1.09	1.823	0.139	0.853	0.024	0.338	1.60	1.033	▽
	1.202	1.200	.720	.101	.248	2.8	-1.99	1.721	.099	.980	.002	.357	1.40	.936	
	1.193	1.342	.776	.138	.314	3.0	-1.79	1.720	.098	.710	.040	.407	1.59	1.066	
	1.100	1.226	.813	.082	.211	2.0	-2.79	1.617	.060	.732	.022	.422	1.495	1.041	
H-18	1.250		0.772	0.146	0.325	4.5	-0.49	1.782	0.123	0.842	0.023	0.397	1.589	1.040	▷
	1.160	1.388	.822	.113	.342	4.0	-.99	1.689	.085	.752	.028	.431	1.646	1.115	
	1.070	1.277	.855	.075	.249	2.9	-2.08	1.591	.051	.680	.024	.412	1.565	1.101	
H-50	1.072	1.459	0.852	0.119	0.340	7.8	1.8	1.668	0.087	0.583	0.052	0.554	1.770	1.208	◁
	1.000	1.430	.937	.050	.327	7.0	1.0	1.615	.048	.920	.004	.604	1.800	1.258	
I-10	1.265	1.725	0.648	0.354	0.660	2.97	-1.82	2.02	0.194	0.548	0.160	0.481	2.44	1.487	◇
	1.381	1.788	.566	.447	.623	3.56	-1.23	2.16	.258	.577	.189	.398	2.235	1.312	
	1.134	1.656	.761	.233	.641	2.62	-2.17	1.89	.135	.580	.098	.576	2.460	1.555	
	1.154	1.607	.760	.219	.589	1.35	-3.14	1.86	.130	.594	.089	.510	2.185	1.392	

TABLE II. - Concluded. SUMMARY DATA FOR TRANSONIC ROTORS

Rotor	Inlet relative Mach number, M_1	Total-pressure ratio, P_2/P_1	Adiabatic efficiency, η_{ad}	Measured loss coefficient, $\bar{\omega}$	Diffusion factor, D	Incidence angle, deg		Suction-surface Mach number, M_s	Shock-loss coefficient, $\bar{\omega}_s$	Loss ratio, $\bar{\omega}_s/\bar{\omega}$	Profile loss, $\bar{\omega} - \bar{\omega}_s$	$\left(\frac{\Delta p}{q}\right)_{M_s}$	V_s/V_2	V_0/V_2	Data-point symbol
						i	i_s								
I-20	1.215	1.841	0.743	0.270	0.588	3.75	-0.97	1.992	0.178	0.659	0.092	0.509	2.195	1.349	D
	1.198	1.827	.725	.285	.631	5.0	.28	2.022	.185	.649	.100	-----	2.380	1.446	
	1.330	1.915	.655	.362	.610	4.52	-.20	2.133	.241	.666	.121	.402	2.210	1.309	
	1.115	1.693	.[illegible]	.120	.513	1.6	-3.12	1.854	.116	.967	.004	.575	2.055	1.324	
	1.100	1.715	.674	.120	.556	3.0	-1.12	1.872	.124	1.003	-.004	-----	2.265	1.445	
I-40	1.134	1.991	0.868	0.160	0.539	4.88	-0.86	1.952	0.147	0.919	0.013	0.539	2.042	1.277	◇
	1.135	2.051	.871	.164	.515	5.28	-.28	1.948	.152	.927	.012	-----	2.040	1.268	
	1.250	2.195	.772	.335	.523	4.71	-.83	2.027	.195	.582	.140	.466	1.860	1.151	
	1.244	2.103	.750	.320	.568	5.32	-.22	2.043	.199	.622	.121	.464	1.838	1.174	
	1.042	1.781	.957	.045	.478	2.90	-2.64	1.805	.096	2.133	-.051	.581	2.020	1.308	
	1.020	1.776	.965	.039	.544	4.32	-1.22	1.846	.104	2.667	-.065	.633	2.260	1.451	
I-50	1.086	2.035	0.905	0.131	0.510	5.30	-1.14	1.887	0.126	0.962	0.005	0.562	2.07	1.312	◇
	1.077	2.070	.904	.131	.460	5.70	-.74	1.895	.127	.969	.004	.601	2.13	1.355	
	1.194	2.284	.802	.287	.495	5.40	-1.04	1.973	.169	.589	.118	.437	1.83	1.132	
	1.186	2.227	.778	.319	.521	5.90	-.54	1.986	.172	.539	.147	.485	1.885	1.158	
I-60	1.028	2.072	0.928	0.105	0.463	5.80	-0.62	1.887	0.106	1.010	-0.001	0.595	1.985	1.273	◇
	1.019	2.011	.925	.110	.504	6.27	-.15	1.895	.108	.982	.002	.636	2.090	1.333	
	1.126	2.342	.850	.280	.454	6.10	-.32	1.973	.141	.504	.139	.451	1.840	1.156	
	1.122	2.223	.808	.280	.472	6.60	.18	1.986	.145	.558	.115	.514	1.870	1.167	
J-10	1.080	1.235	0.782	0.107	0.523	4.06	-1.48	1.528	0.041	0.383	0.066	0.460	1.632	1.183	◁
	1.074	1.271	.843	.082	.373	4.23	-1.29	1.530	.041	.500	.041	.488	1.704	1.232	
	1.053	1.326	.861	.086	.427	5.51	-.01	1.562	.044	.512	.042	.542	1.842	1.313	
J-16	1.056	1.229	0.791	0.102	0.312	4.10	-1.66	1.517	0.036	0.353	0.066	0.482	1.650	1.198	◀
	1.050	1.259	.841	.083	.364	4.23	-1.53	1.518	.036	.434	.047	.508	1.730	1.253	
	1.028	1.325	.890	.067	.414	5.55	-.21	1.554	.039	.582	.028	.564	1.858	1.327	
K-10	1.088	1.220	0.753	0.117	0.348	3.92	-1.80	1.634	0.052	0.530	0.055	0.465	1.687	1.169	⌂
	1.076	1.245	.761	.131	.391	4.66	-.86	1.652	.054	.489	.067	.500	1.775	1.221	
	1.066	1.265	.781	.121	.407	4.85	-.67	1.652	.053	.521	.058	.520	1.810	1.246	
K-16	1.084	1.213	0.753	0.117	0.352	3.88	-1.90	1.651	0.058	0.486	0.059	0.490	1.705	1.182	◆
	1.052	1.257	.755	.129	.368	4.62	-1.14	1.651	.061	.473	.068	.520	1.786	1.227	
	1.042	1.256	.784	.119	.392	4.80	-.96	1.652	.060	.504	.059	.542	1.865	1.158	
L-10	1.082	1.213	0.700	0.148	0.340	4.05	-1.47	1.781	0.096	0.649	0.052	0.500	1.740	1.142	D
	1.074	1.203	.718	.133	.328	4.14	-1.38	1.780	.095	.714	.038	.489	1.724	1.130	
L-16	1.081	1.216	0.732	0.133	0.346	3.82	-1.94	1.775	0.091	0.684	0.042	0.518	1.773	1.164	▶
	1.050	1.204	.744	.121	.324	4.14	-1.62	1.781	.091	.752	.030	.508	1.754	1.148	
M-10	1.019	1.415	0.789	0.173	0.500	5.35	0.43	1.675	0.061	0.353	0.112	0.627	2.105	1.436	□
	1.038	1.549	.785	.151	.407	4.01	-.91	1.657	.056	.371	.095	.566	1.88	1.299	
	1.026	1.392	.813	.143	.478	4.66	-.26	1.654	.058	.406	.085	.602	2.03	1.394	
	1.093	1.288	.750	.146	.519	3.86	-1.26	1.654	.067	.459	.079	.474	1.677	1.152	
	1.086	1.328	.762	.154	.571	4.16	-.76	1.667	.069	.448	.085	.444	1.775	1.209	
N-10	1.018	1.315	0.926	0.043	0.276	4.2	-0.71	1.687	0.064	1.488	-0.021	-----	1.505	1.006	×
	1.020	1.352	.929	.045	.325	4.9	-.01	1.712	.070	1.556	-.025	0.385	1.839	1.213	
	1.037	1.408	.887	.082	.380	5.73	.82	1.746	.081	.988	.001	.532	1.520	1.031	
O-16	1.135	1.327	0.786	0.128	0.338	2.6	-2.27	1.632	0.069	0.539	0.059	0.481	1.670	1.156	▷
	1.133	1.308	.763	.138	.329	2.5	-2.37	1.627	.067	.486	.071	.475	1.664	1.154	
O-25	1.097	1.346	0.755	0.185	0.350	2.9	-2.17	1.610	0.059	0.358	0.106	0.513	1.727	1.206	▽
	1.095	1.344	.797	.130	.336	2.8	-2.27	1.606	.058	.446	.072	.507	1.699	1.189	
O-33	1.082	1.377	0.816	0.130	0.362	2.8	-2.48	1.588	0.049	0.377	0.081	0.547	1.767	1.246	◁
	1.080	1.359	.847	.106	.347	2.7	-2.58	1.583	.048	.453	.058	.542	1.742	1.231	
P-16	1.108	1.532	0.802	0.174	0.488	2.5	-2.39	1.608	0.060	0.345	0.114	0.550	1.955	1.367	△
P-25	1.100	1.503	.820	.152	.482	.8	-4.27	1.548	.047	.309	.105	.548	1.918	1.375	▽
P-33	1.083	1.509	.870	.107	.484	.7	-4.59	1.536	.045	.402	.064	.540	1.933	1.394	▷
P-50	1.049	1.483	.854	.118	.476	-1.3	-7.06	1.458	.027	.229	.091	.567	1.924	1.438	◁
Q-9	1.061	1.310	0.848	0.089	0.340	1.25	-5.90	1.767	0.089	1.000	0.000	0.492	1.760	1.160	◇
	1.058	1.353	.893	.067	.394	1.40	-5.75	1.770	.089	1.328	-.022	.524	1.85	1.216	
	1.055	1.377	.909	.059	.402	1.78	-5.37	1.782	.092	1.559	-.033	.544	1.877	1.230	
	1.049	1.401	.929	.048	.424	2.31	-4.84	1.797	.095	1.979	-.047	.560	1.930	1.257	
R-9	1.056	1.309	0.815	0.113	0.405	3.0	-4.15	2.15	0.208	1.837	-0.195	0.542	2.22	1.307	◿
S-9	1.058	1.323	0.858	0.088	0.329	2.89	-4.26	1.95	0.142	1.652	-0.056	0.583	1.85	1.148	+
	1.165	1.270	.720	.149	.221	3.37	-3.78	2.05	.189	1.268	.040	.257	1.58	.986	
	1.258	1.309	.680	.183	.239	4.45	-2.70	2.18	.245	1.338	.162	.219	1.565	.917	

[redacted]

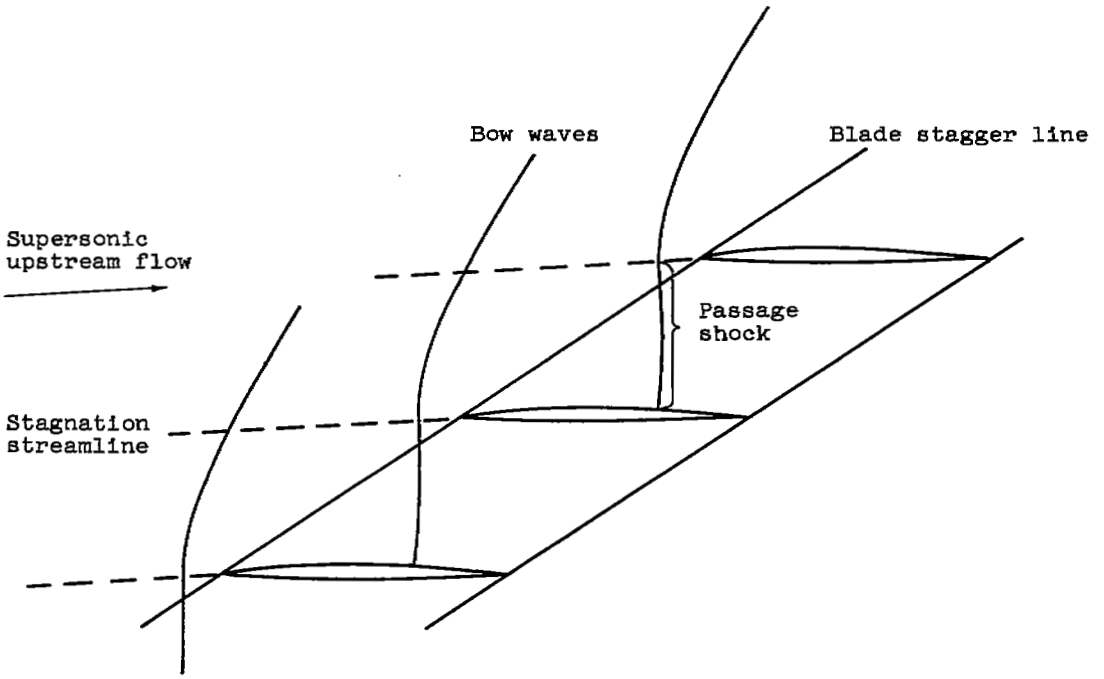

Figure 1. - Shock-wave configuration in cascade of airfoils at supersonic inlet relative Mach number.

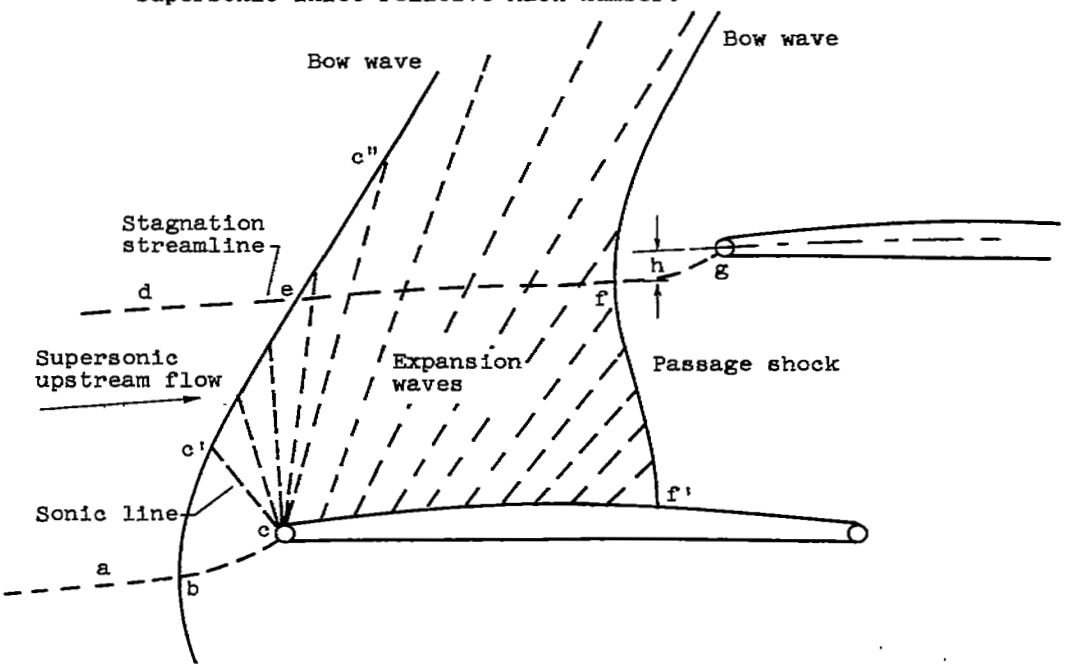

Figure 2. - Details of flow field at inlet of cascade of airfoils operated with supersonic inlet relative Mach number.

[redacted]

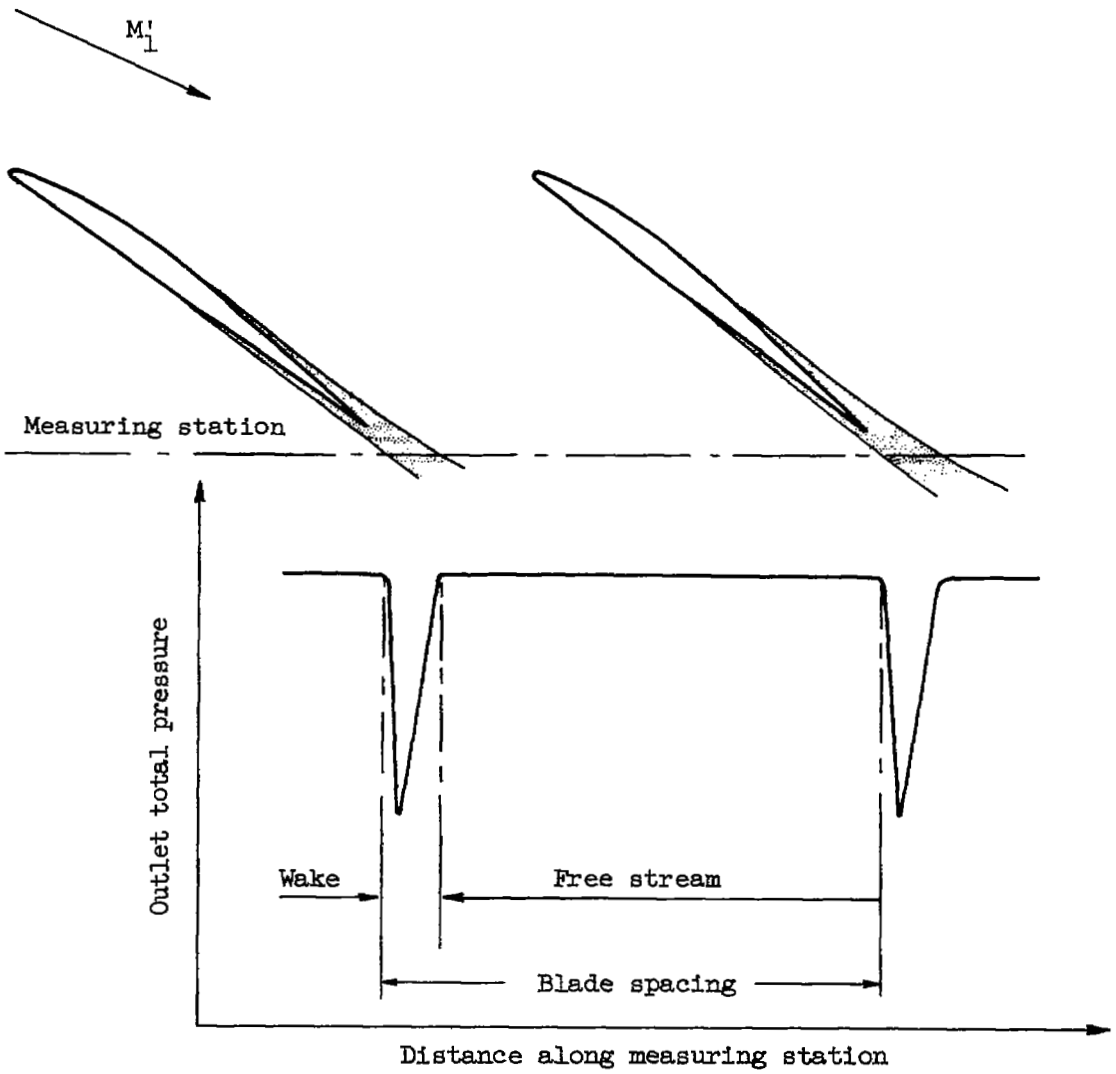

Figure 3. - Variation of total pressure downstream of low-speed cascade.

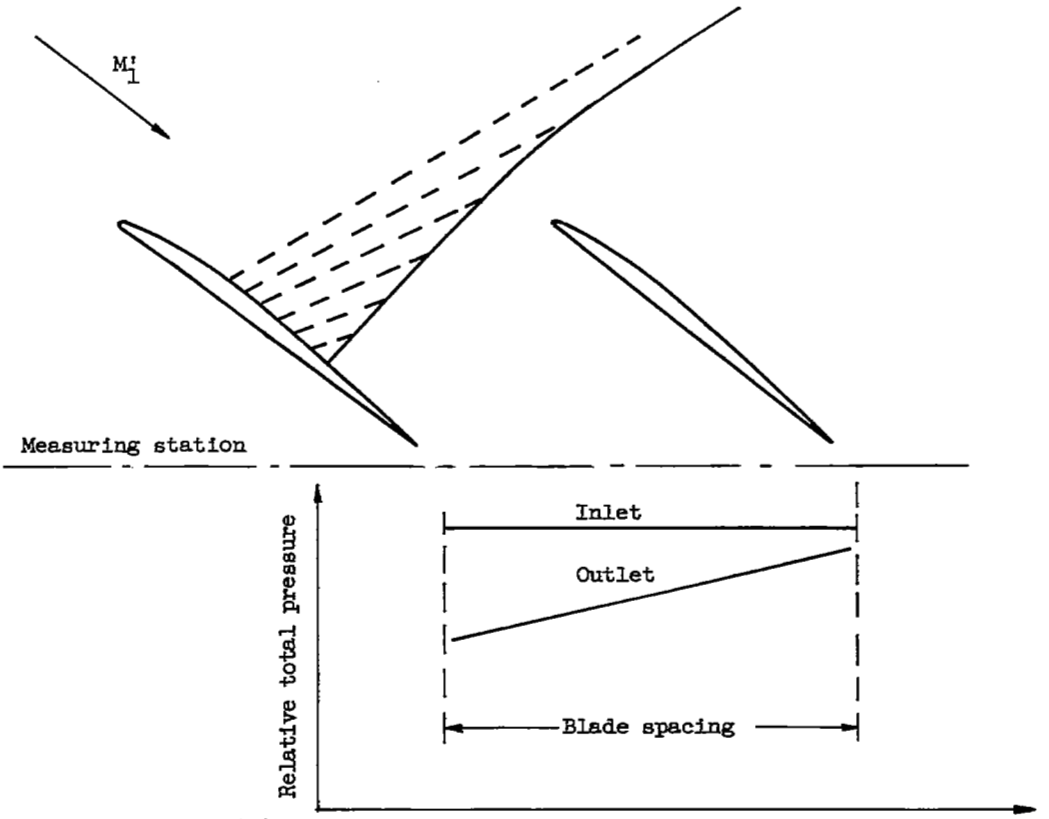

(a) Variation caused by passage shock.

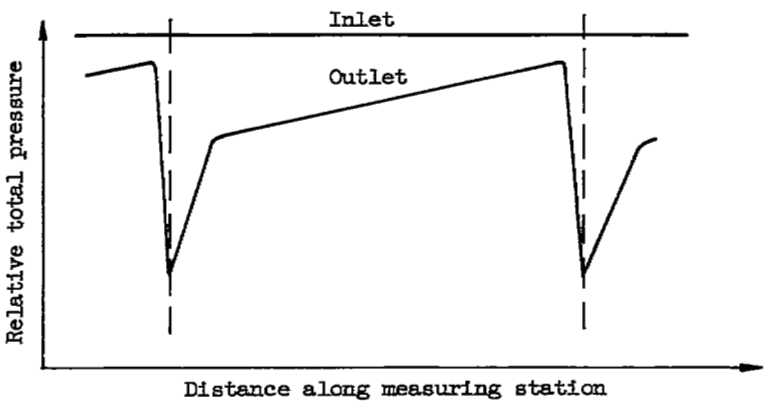

(b) Variation caused by passage shock and viscous effects.

Figure 4. - Circumferential variation of relative total pressure at outlet of blade element operating with supersonic inlet relative Mach numbers.

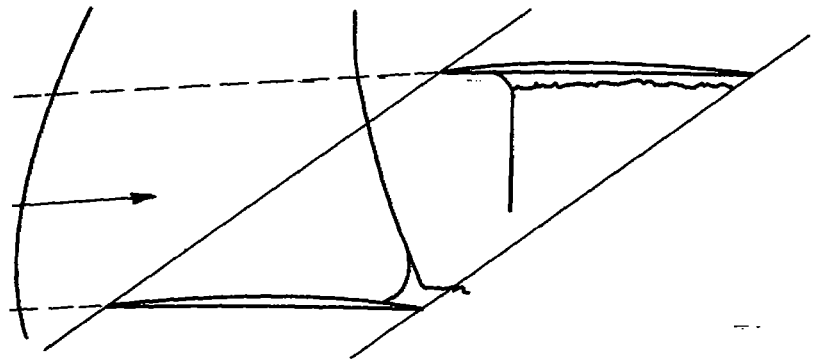

(a) Low back pressure (point A).

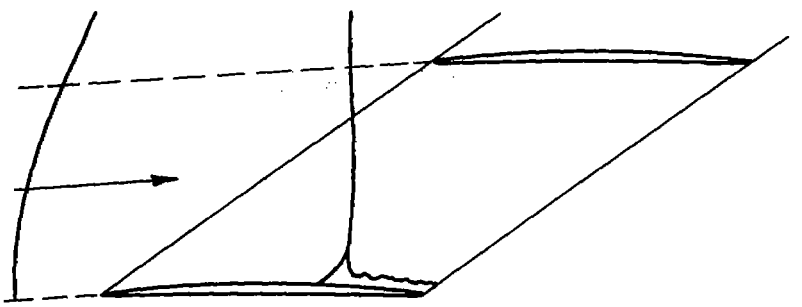

(b) Moderate back pressure (point B near peak efficiency).

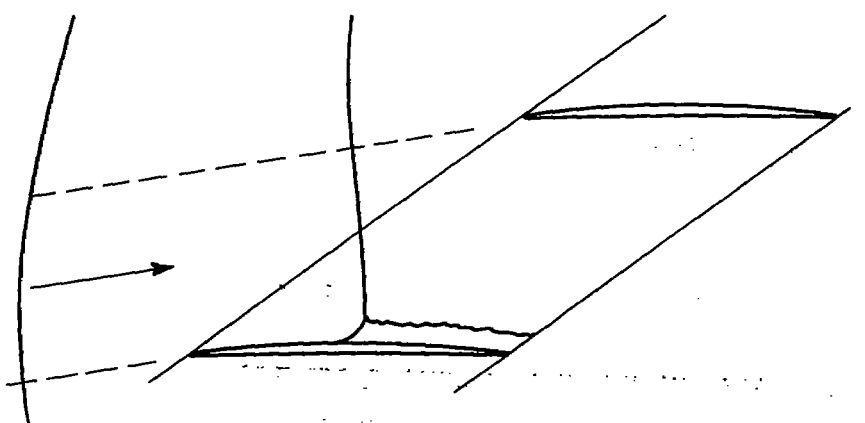

(c) High back pressure (point C).

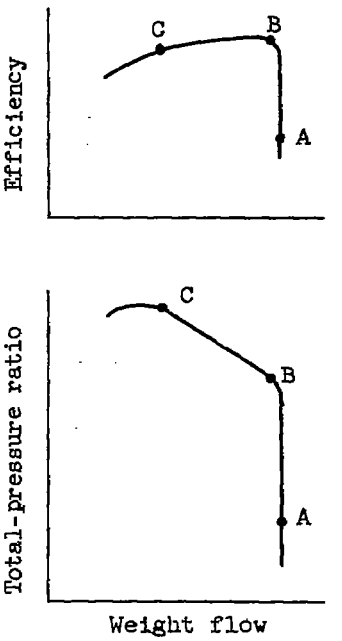

Figure 5. - Variation of passage shock with back pressure (operation at supersonic inlet relative Mach number).

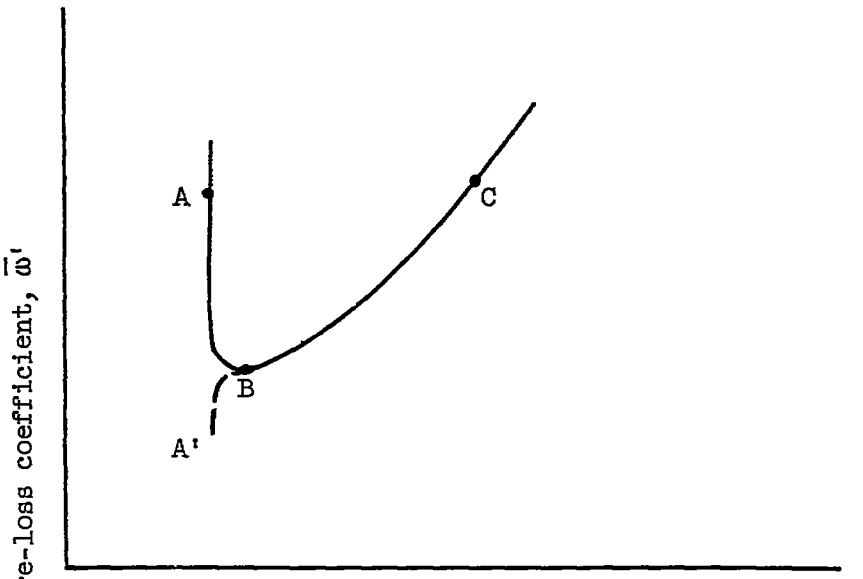

(a) Variation with incidence angle.

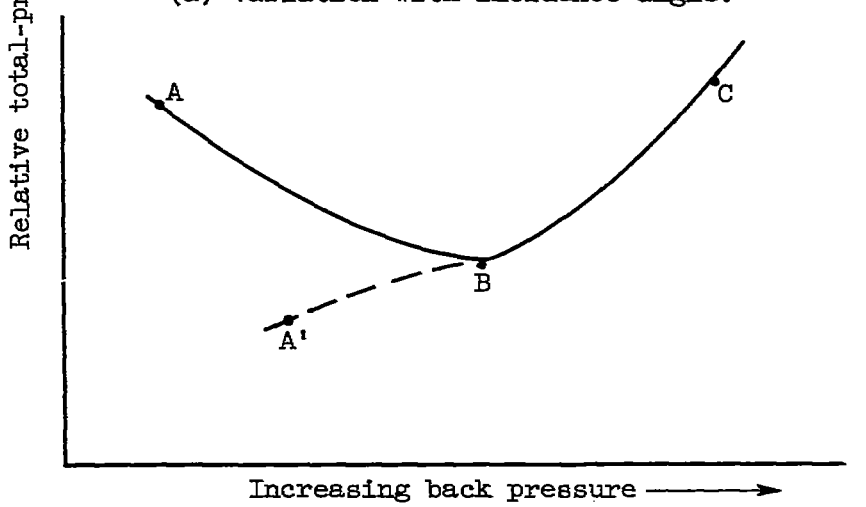

(b) Variation with back pressure.

Figure 6. - Typical measured variations of blade-element losses with incidence angle and back pressure for operation with supersonic inlet relative Mach number.

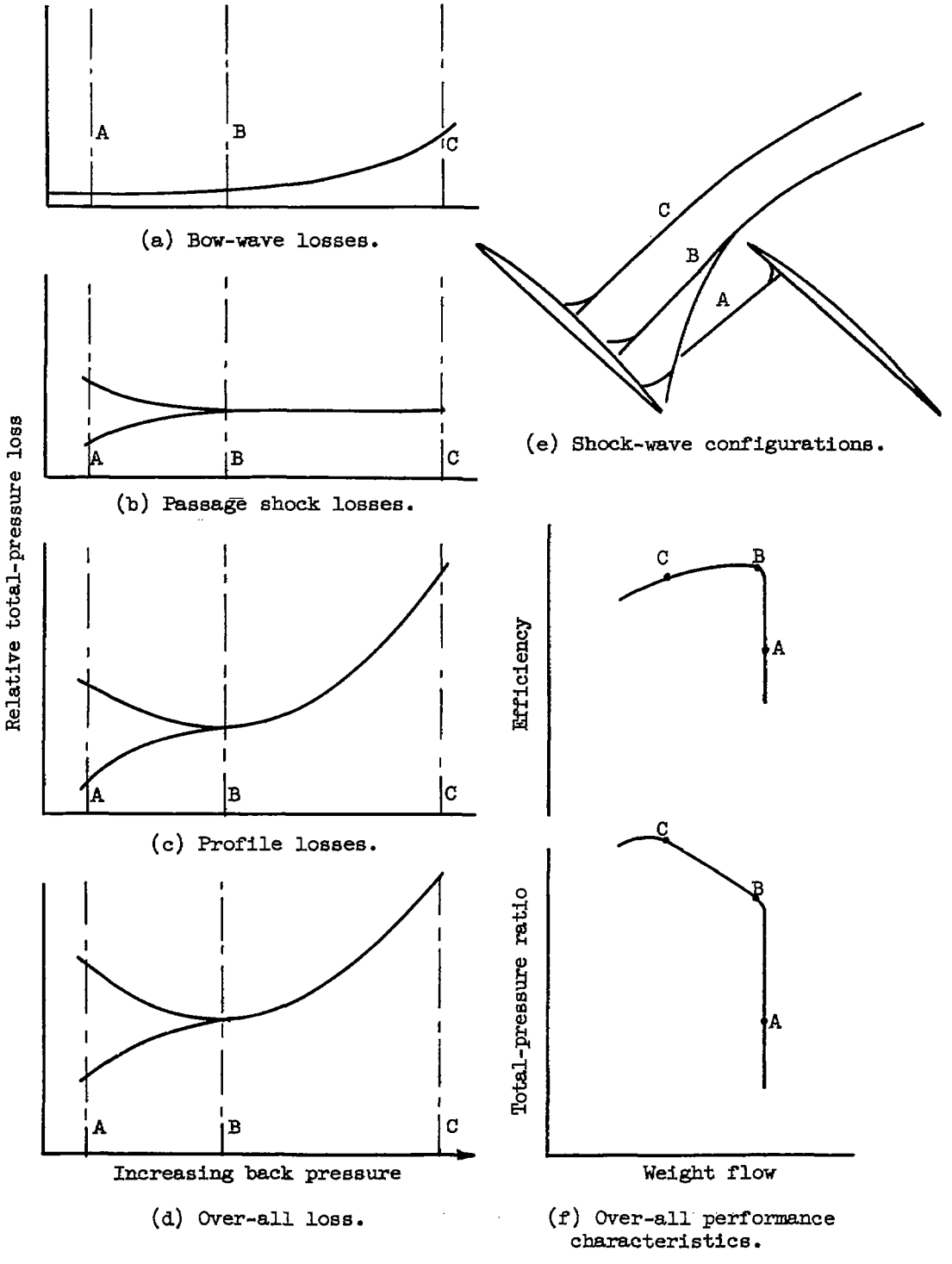

Figure 7. - Blade-element loss variations deduced from flow model.

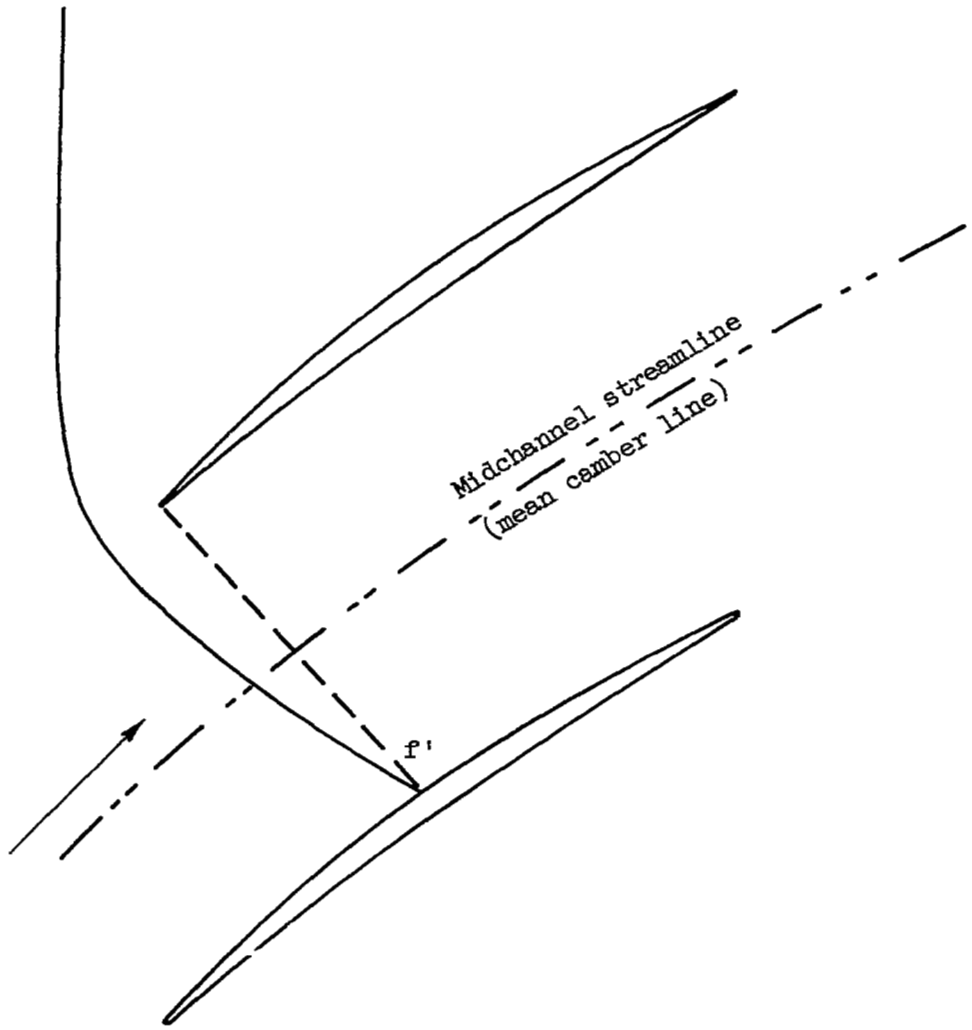

Figure 8. - Passage shock-wave approximation for estimating shock-loss levels.

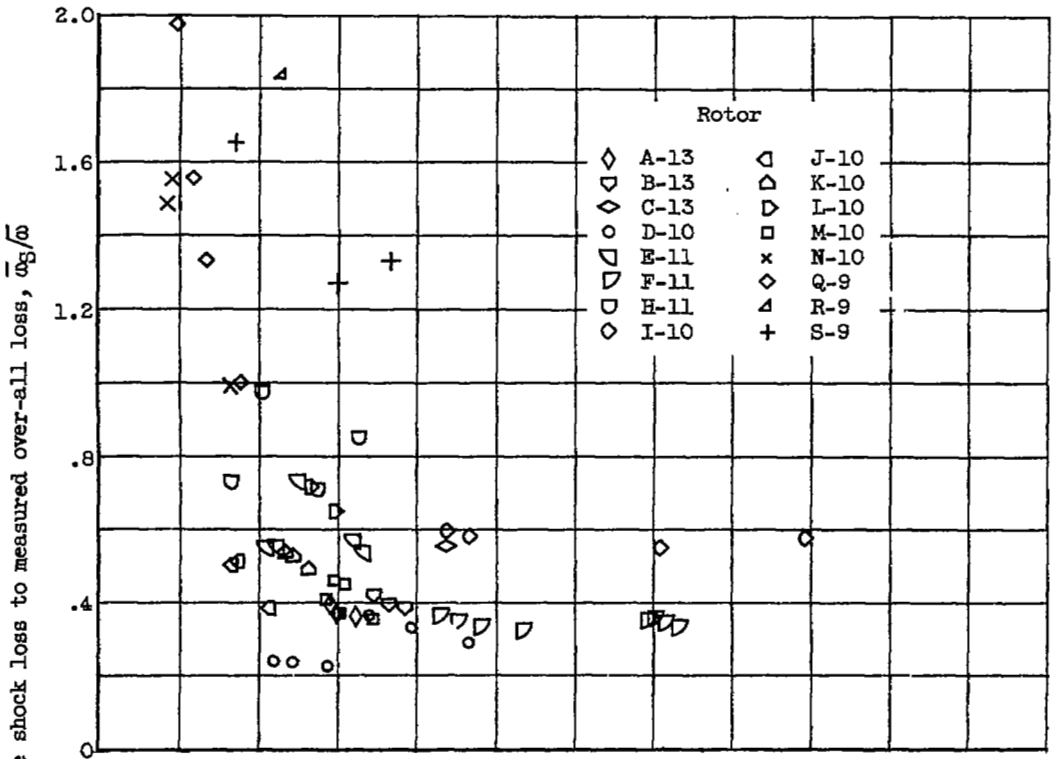

(a) Tip section, 13 percent or less of passage height from outer wall.

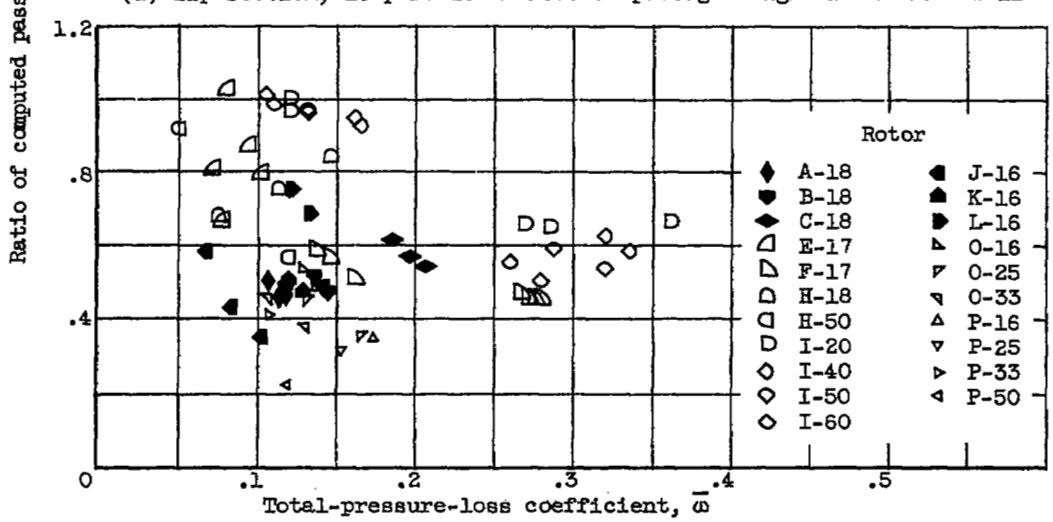

Ratio of computed passage shock loss to measured over-all loss, $\bar{\omega}_S/\bar{\omega}$

(b) Blade-element sections located 16 to 60 percent of passage height from outer wall.

Figure 9. - Ratio of computed passage shock loss to measured over-all loss for blade elements.

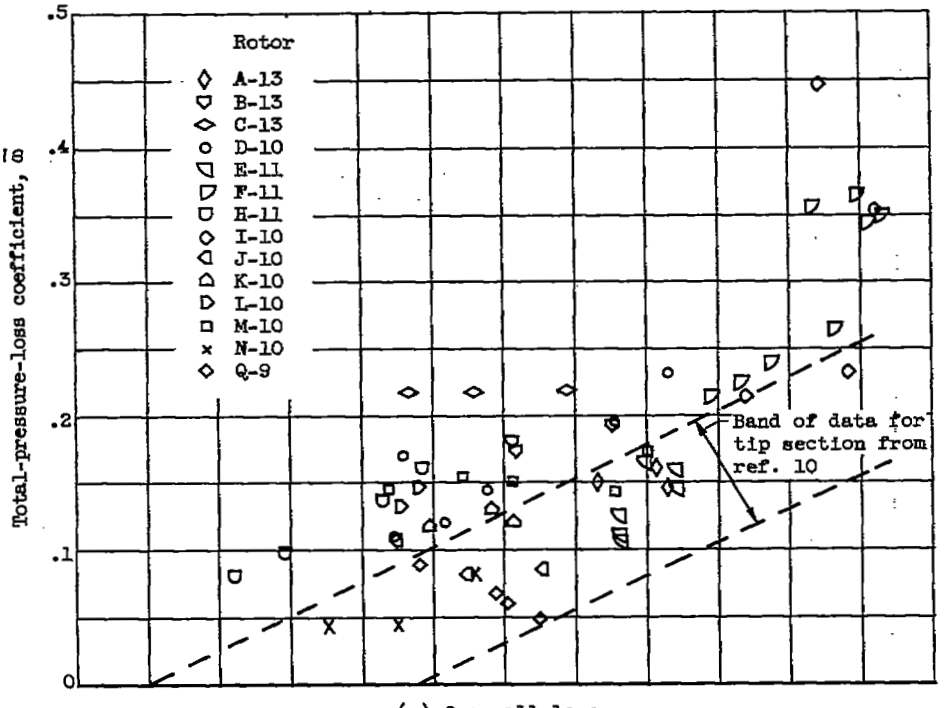

(a) Over-all loss.

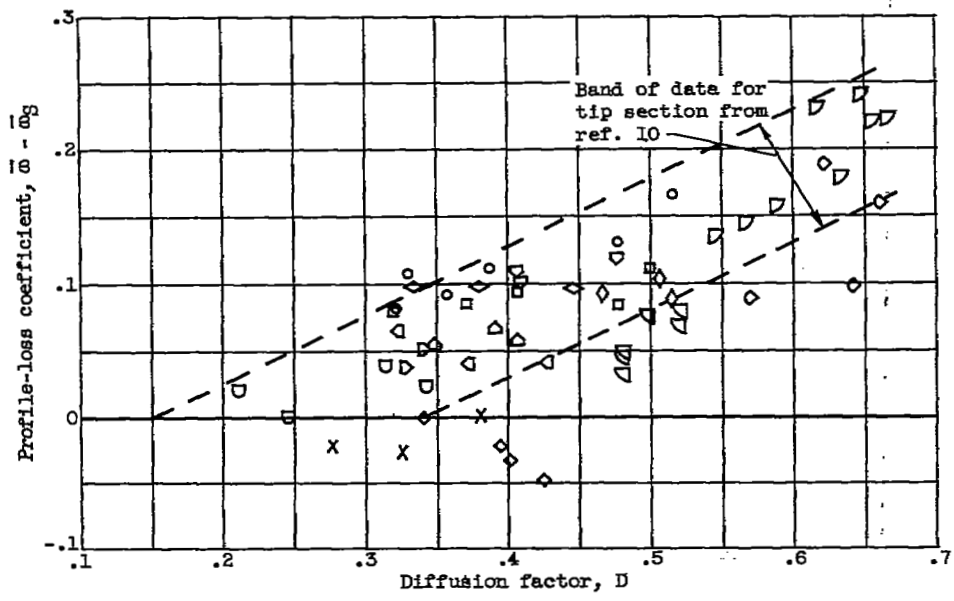

(b) Profile loss.

Figure 10. - Variation of over-all and profile losses with diffusion factor for several transonic-compressor rotors. Tip section, 13 percent of passage height or less from outer wall.

[redacted]

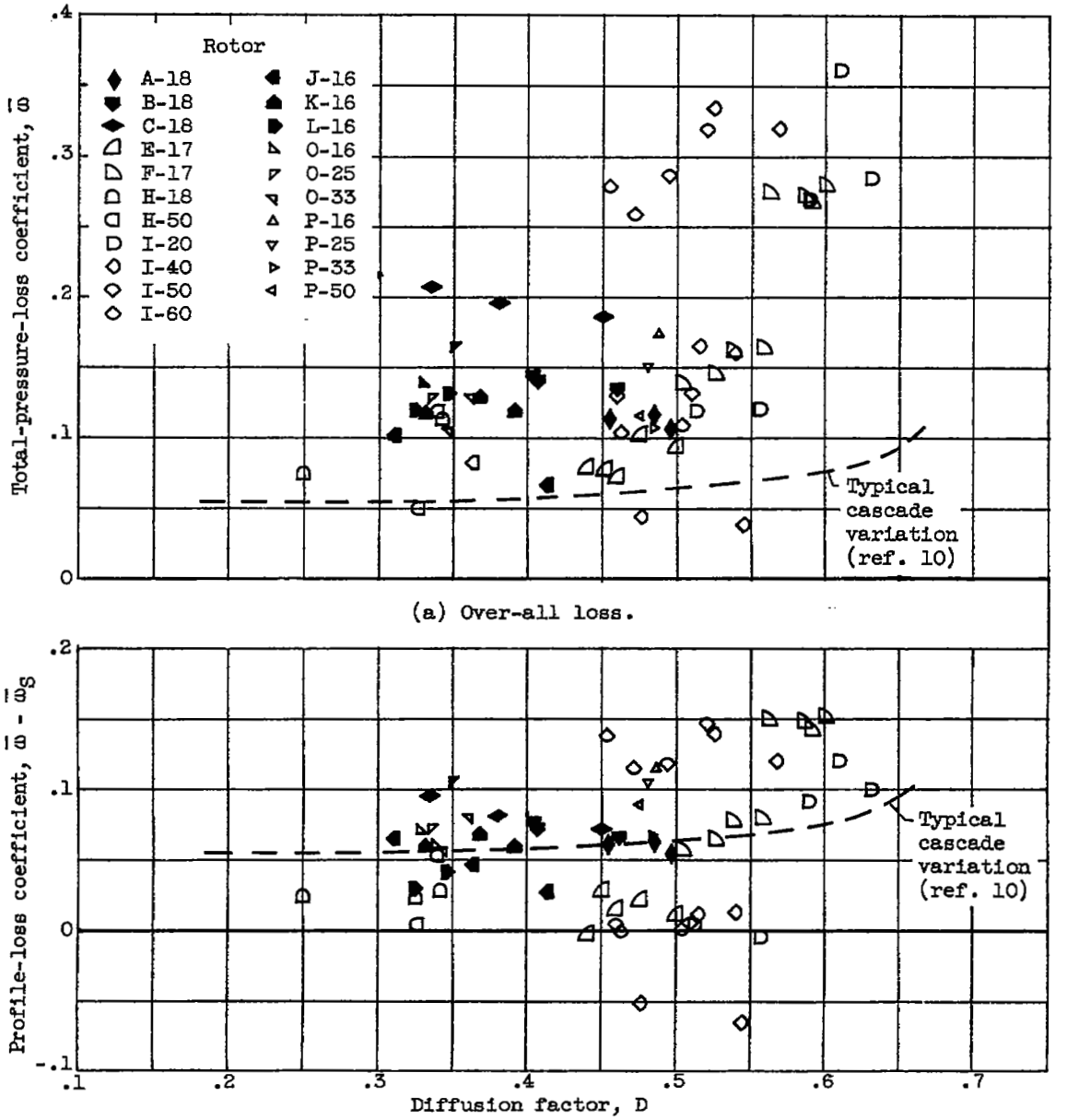

Figure 11. - Variation of over-all and profile loss with diffusion factor for several transonic-compressor rotors at blade-element sections located 16 to 60 percent of passage height from outer wall.

[redacted]

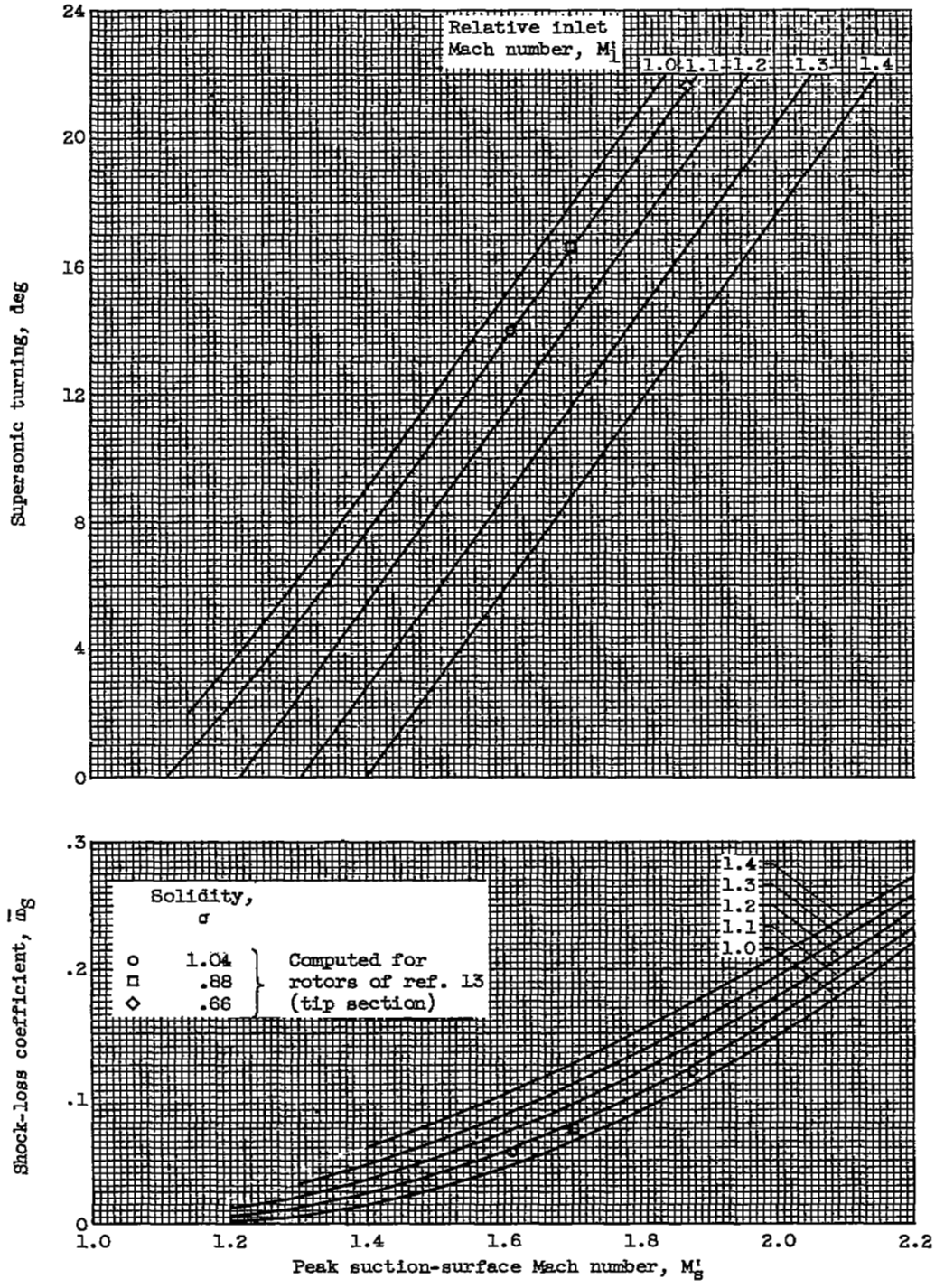

Figure 12. - Computed shock loss and supersonic turning variation with peak suction-surface Mach number.

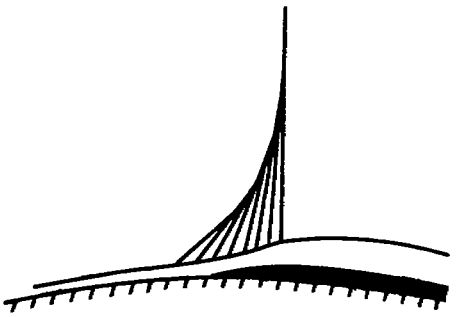

(a) Separation of boundary layer.

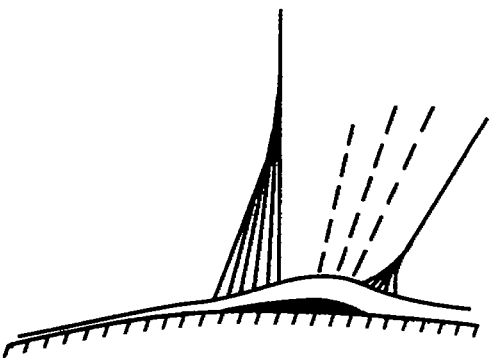

(b) Separation with reattachment.

Figure 13. - Shock - boundary-layer interaction.

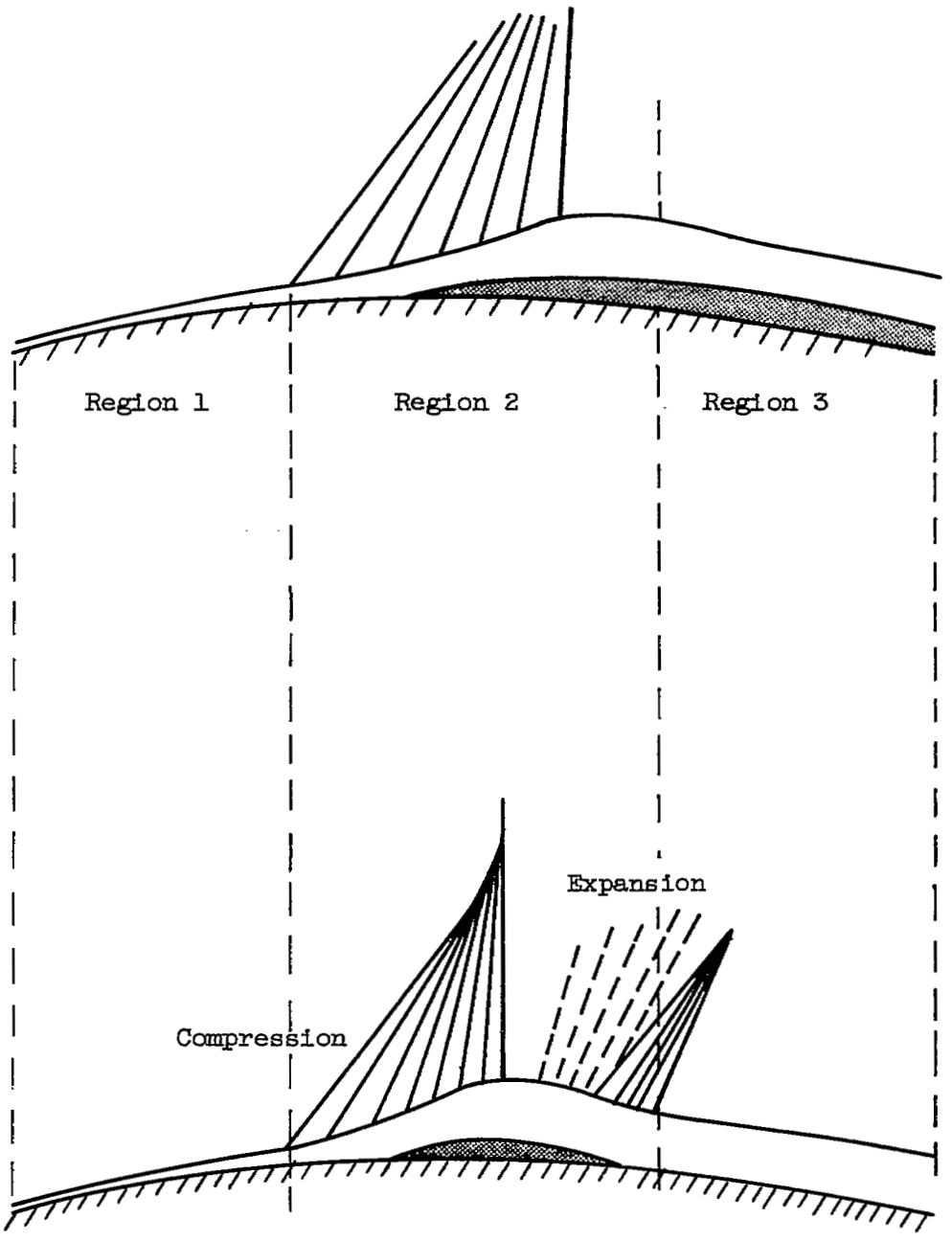

Figure 14. - Two forms of shock - boundary-layer interaction on a compressor blade surface.

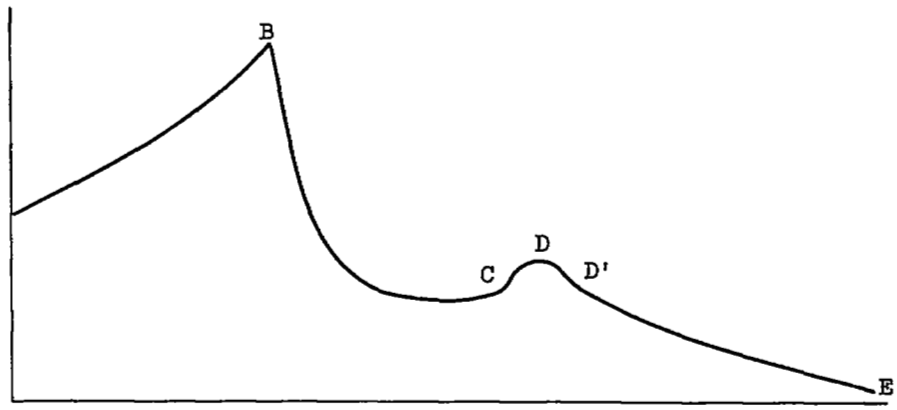

(a) Shock - boundary-layer interaction with expansion downstream followed by compression shock.

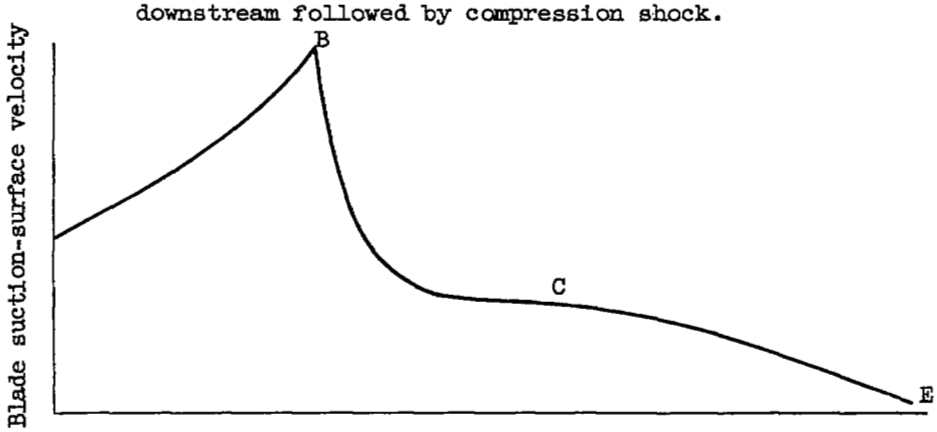

(b) Shock - boundary-layer interaction with subsonic diffusion.

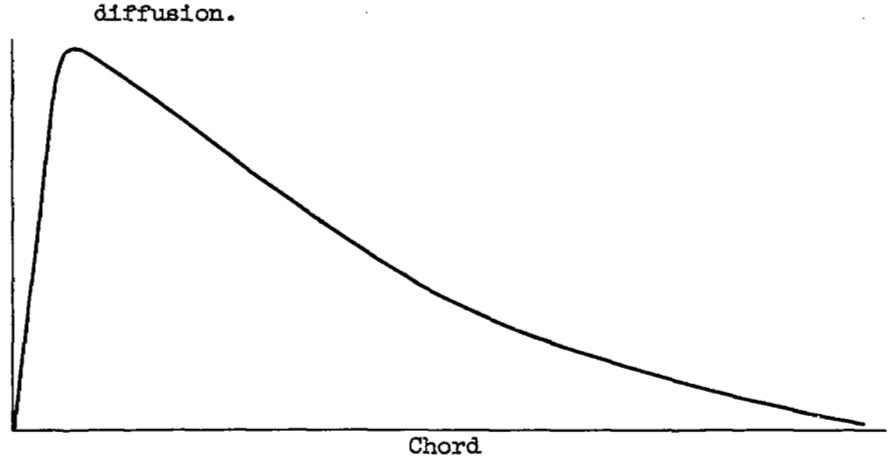

(c) Subsonic velocity profile.

Figure 15. - Compressor blade suction-surface velocity profiles.

[redacted]

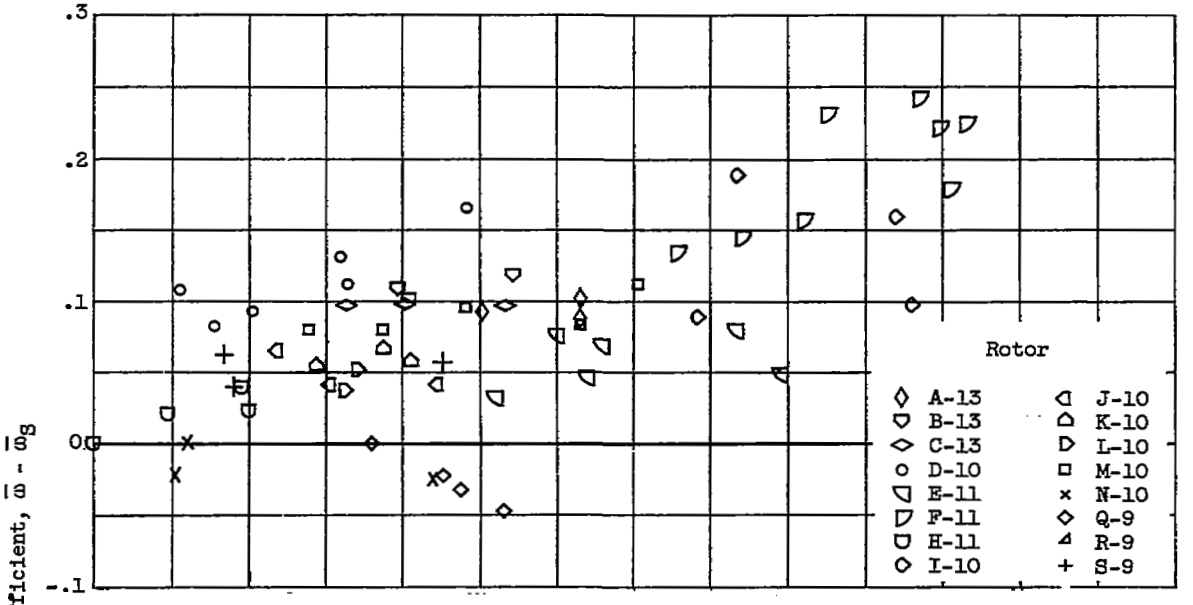

(a) Tip section, 13 percent or less of passage height from outer wall.

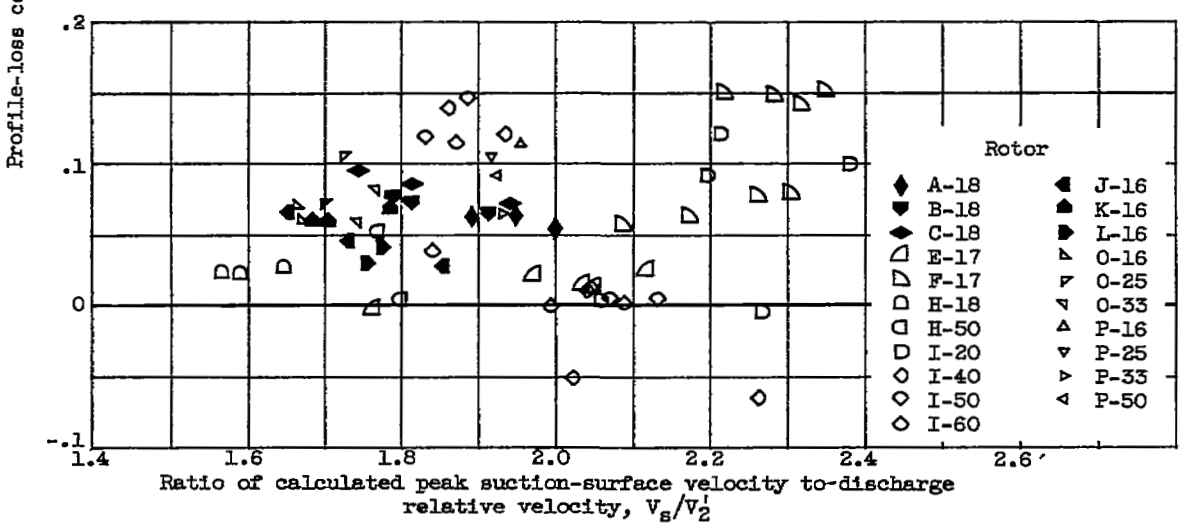

(b) Blade-element sections located 16 to 60 percent of passage height from outer wall.

Figure 16. - Variation of estimated profile loss with ratio of peak suction-surface to discharge velocity.

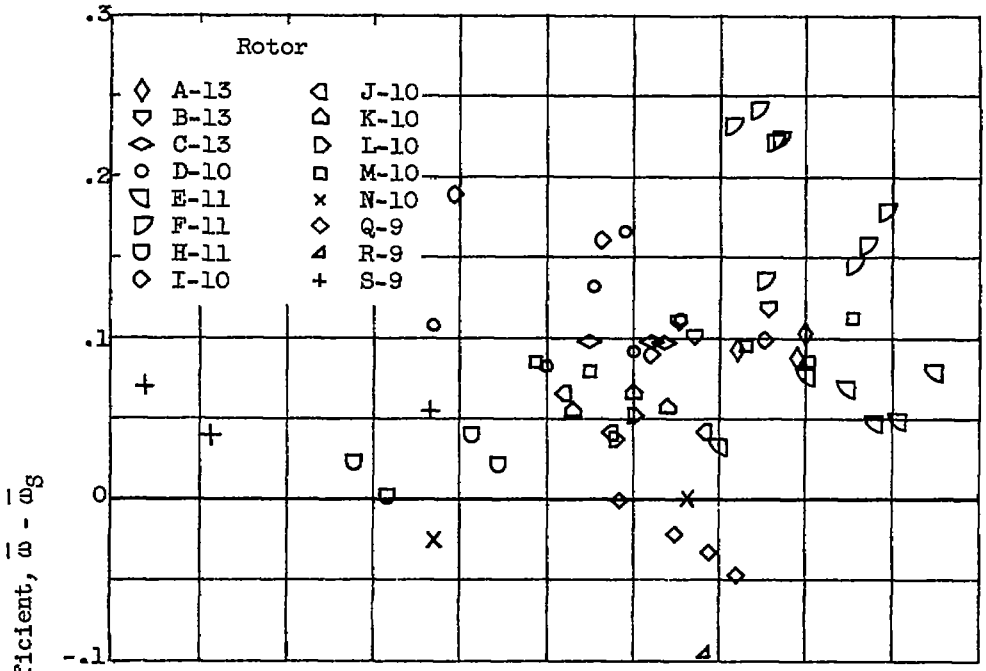

(a) Tip section, 13 percent or less of passage height from outer wall.

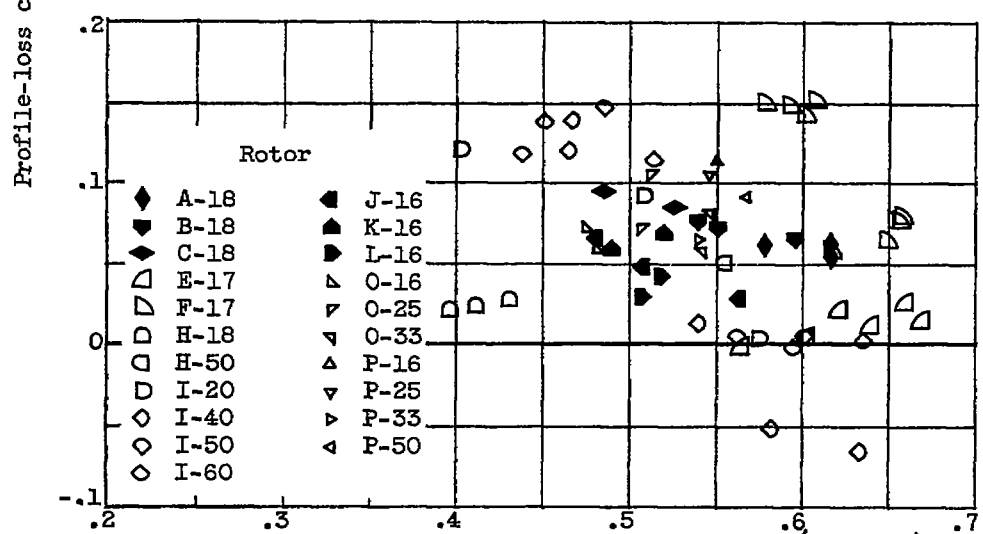

Profile-loss coefficient, $\bar{\omega} - \bar{\omega}_s$

Calculated static-pressure-rise coefficient, $\frac{(p_2 - p_s)}{p_1' - p_s}$

(b) Blade-element sections located 16 to 60 percent of passage height from outer wall.

Figure 17. - Variation of estimated profile loss with static-pressure-rise coefficient.

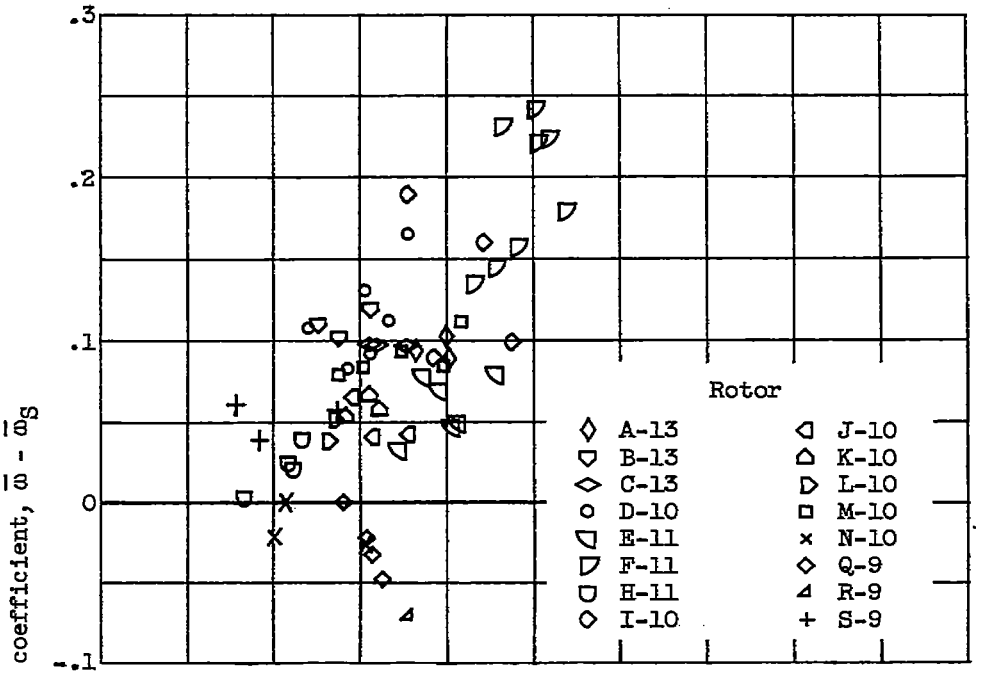

(a) Tip section, 13 percent or less of passage height from outer wall.

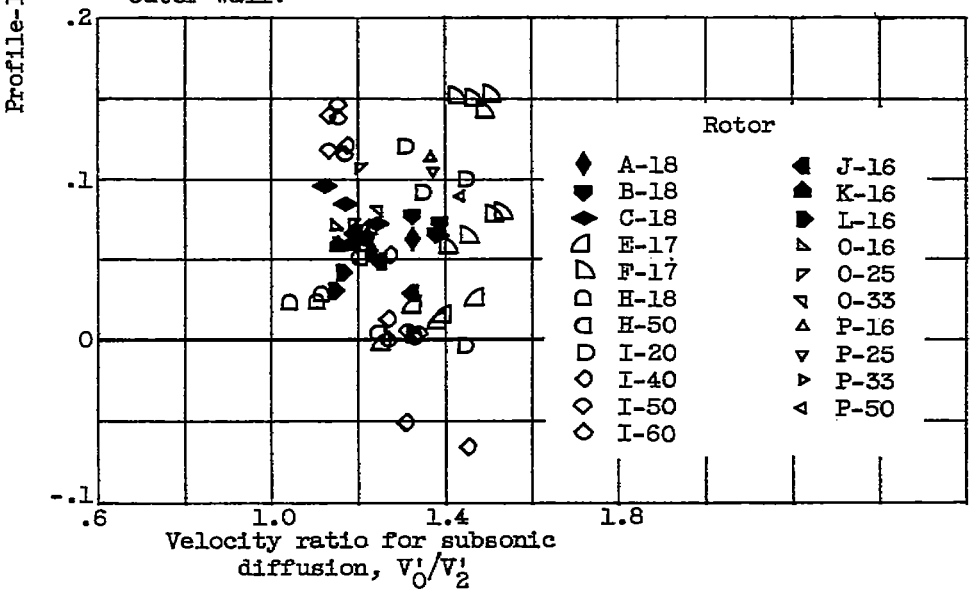

(b) Blade-element sections located 16 to 60 percent of passage height from outer wall.

Figure 18. - Variation of profile losses with velocity ratio for subsonic diffusion.

[redacted]

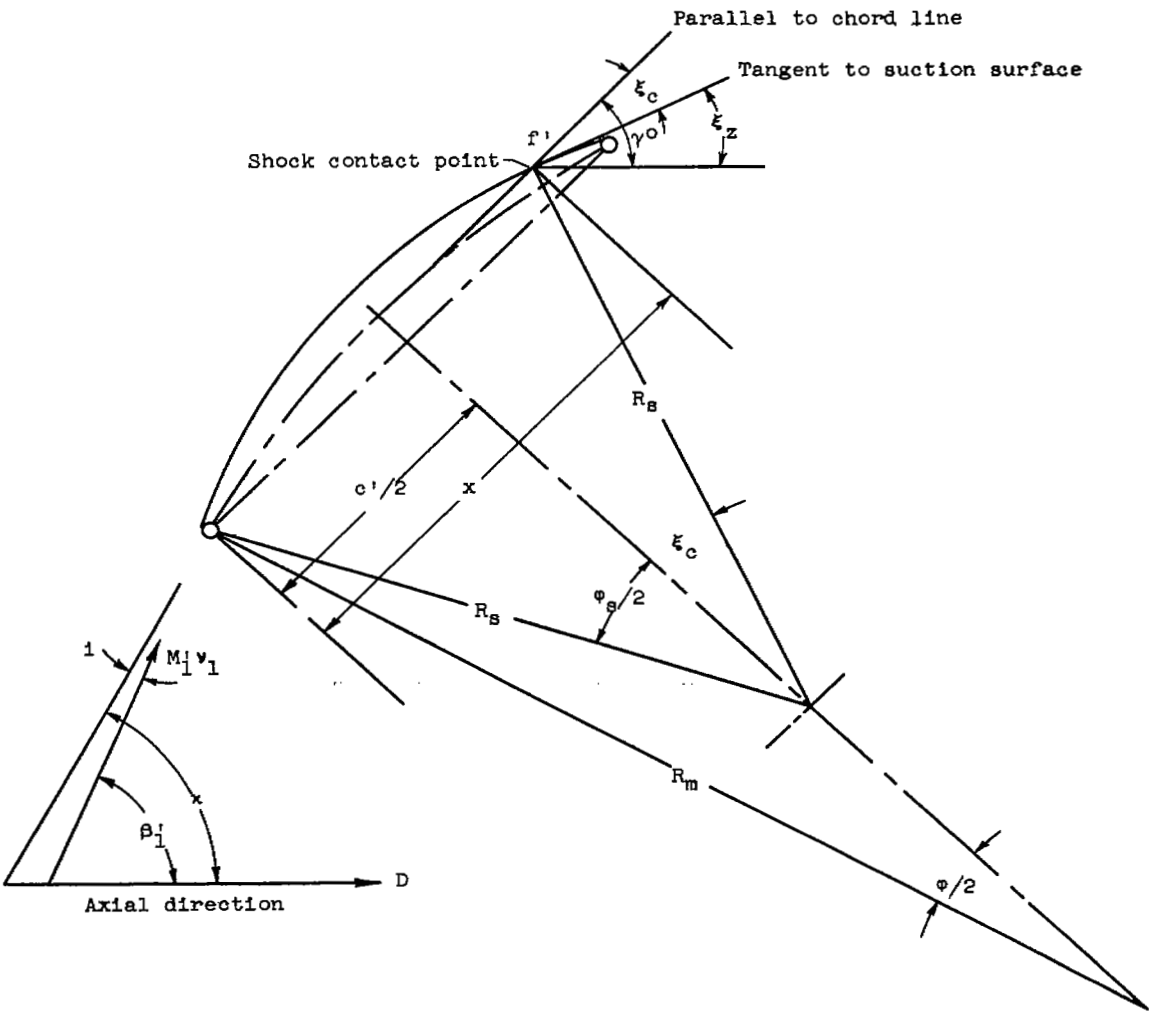

Figure 19. - Circular-arc-blade geometry.

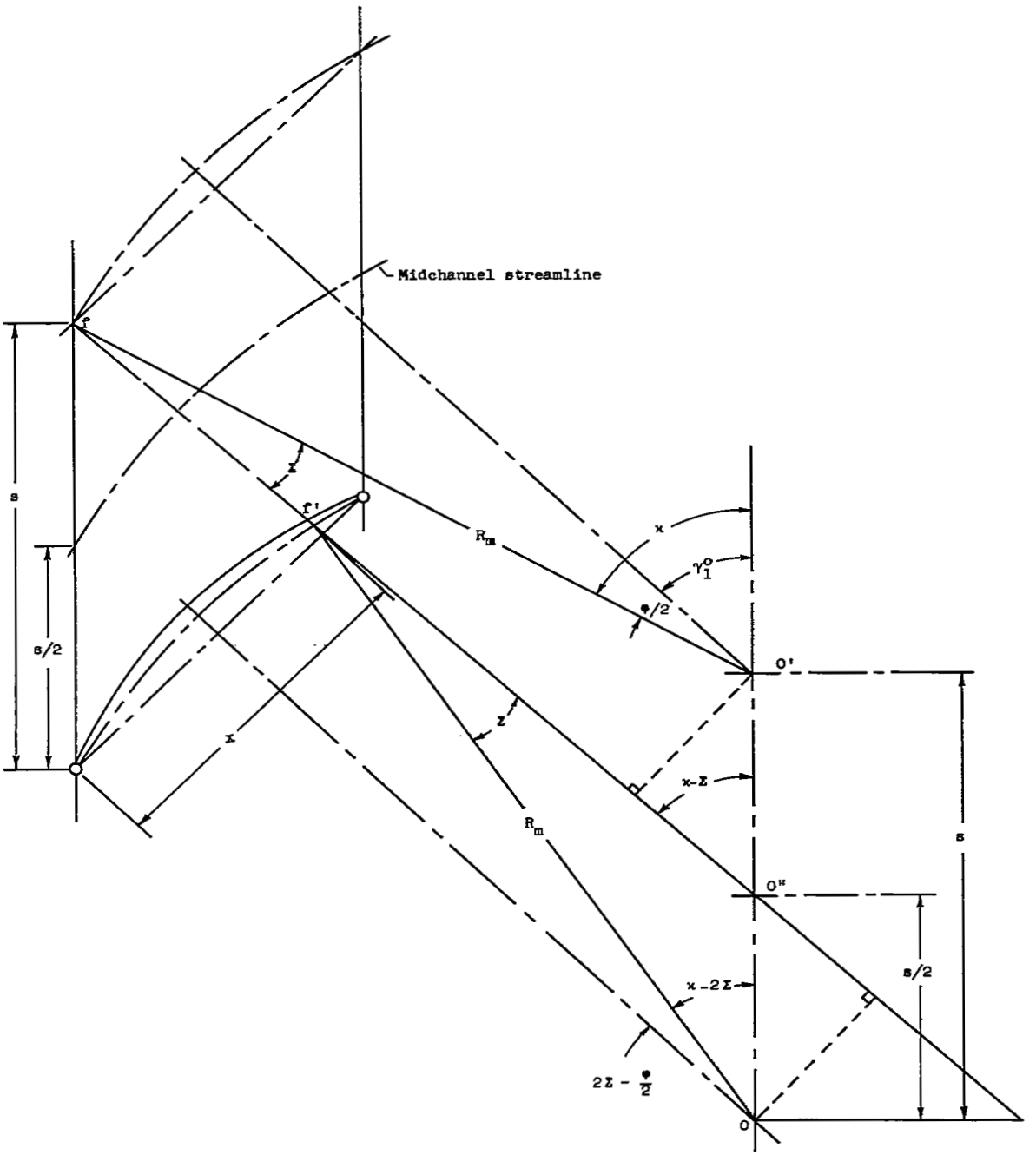

Figure 20. - Shock location and blade geometry.